

POLITECNICO DI TORINO

MSc in Mechatronic Engineering

Master's Thesis

Drag Free Control Design for a space-based Gravitational Wave Observatory



Supervisors:

Prof. Carlo NOVARA

Doc. Simone VIDANO

Candidate:

Agata ZOCCO

July 2020

Acknowledgments

Un ringraziamento al Professore Novara, per avermi proposto e reso partecipe di un progetto interessante quanto impegnativo, grazie per avermi dato la possibilità di accrescere la mia conoscenza conciliando due campi a me cari, l'aerospazio e i controlli.

Un grazie immenso anche a Simone, che con la sua pazienza e immensa disponibilità, mi ha accompagnato in questo percorso. Un riferimento e un sostegno davvero importante.

Grazie alla mia famiglia, che da anni riesce a darmi da lontano tutto quello di cui ho bisogno senza la necessità di dire nulla. Un amore, un sostegno e una forza senza cui non avrei potuto iniziare e tanto meno finire questo percorso.

Grazie alla mia seconda casa qui a Torino, senza casa RT non sarebbe stata la stessa cosa.

Contents

Acknowledgments	I
Introduction	1
1 Description of a space based observatory	3
1.1 System Description	3
1.1.1 System	3
1.1.2 System Reference Frame	7
1.1.3 Dynamics Model: equations	8
1.1.4 Linearization	12
2 Actuators, Sensors and Disturbances	15
2.1 Actuators	15
2.1.1 Micro Propulsion System	15
2.1.2 Gravitational Reference Sensor	16
2.2 Sensors	17
2.2.1 Optical Measurement System	17
2.3 Disturbances	19
3 Mixed Sensitivity Loop Shaping	25
3.1 Mixed Sensitivity Loop Shaping Approach	25
3.1.1 Problem settings	26
3.1.2 Loop shaping approach	27
3.1.3 Mixed sensitivity loop shaping approach	29
3.1.4 Weighting Functions	30
4 Controller Design	35
4.1 Problem setting	35
4.1.1 Performance Requirements	37
4.1.2 Weighting functions choice	38
4.1.3 Example: Drag free control design	46

4.1.4	Controller Semplication	50
5	Simulations	53
5.1	Simulink set	53
5.2	Simulation results	55
5.3	Monte Carlo Simulation and Results	57
6	Conclusions	61

List of Figures

1.1	Spacecraft constellation.[1]	4
1.2	Cutaway view of LISA spacecraft.[2]	4
1.3	Lisa telescope.[3]	5
1.4	SC and TMs Optical Assembly representation.	7
3.1	feedback control system.	26
3.2	Feedback Control System.	27
3.3	Loop shaping.[4]	28
3.4	Augmented Plant.[5]	29
3.5	Weighting Functions.	32
4.1	Control block.	36
4.2	Requirement example.	39
4.3	Augmented Plant.	40
4.4	Feedback control system of the GWs observatory.	41
4.5	Simulink model.	47
4.6	Block scheme.	47
4.7	Sensitivity and Complementary Sensitivity functions.	49
4.8	Drag free loop shape.	49
4.9	Bode Diagram comparison of the reduced controllers.	51
5.1	Simulink scheme.	54
5.2	Drag free position.	55
5.3	TMs position jitter along y and z direction.	56
5.4	Test Mass attitude.	56
5.5	Spacecraft attitude and OA.	57

Introduction

Space applications represent one of the main challenging and interesting environment for Control Engineering. In particular, all satellite systems need some kind of control to carry out their tasks.

In this thesis, H_∞ controllers were designed for Drag-free mode of a scientific spacecraft like LISA. Drag Free means that the control system has to attenuate all the disturbances affecting the scientific experiment according to certain performance requirements.

LISA will be a gravitational waves observatory with a measurement bandwidth lower than the actual ground-based interferometers, such as LIGO and Virgo. It will detect gravitational waves by measuring the relative distance between free falling bodies, known as test masses, by means of a laser interferometer.

It consists of a triangular constellation of three identical spacecraft, orbiting around the Sun at 1AU with an average armlength of $2.5 \cdot 10^6$ Km. Each spacecraft hosts a couple of test masses surrounded by an advanced electrostatic suspension.

LISA aims to observe GWs at frequencies between 0.1 mHz to 100 mHz. If in Drag Free flight it is detected a displacement between the Test Masses, it will be caused by a passing Gravitational Wave.

For what concerns the control design, the initial plant made of 20 inputs and 17 outputs was divided into Multi-Input Multi-Output subsystems, namely the spacecraft attitude and attitude/translation of the two test masses. The output signal are subject to very tight performance requirements in terms of the power spectral densities, that even go down to the nanoscopic scale in case of the test mass translation.

These demanding requirements are difficult to satisfy due to environmental disturbances, actuation and sensing noise. In fact, their values are too high for being

consistent with the performance limits.

A suitable control technique for this application is the H-inf, since it involves in the control design some particular quantities such as the noise and the requirements shapes in the frequency domain. More specifically, three weighting functions are defined. The first one accounts for the reference tracking and disturbance rejections, the second one for the robustness and noise attenuation, the third one to the command activity.

The test masses control worths particular attention. Along the drag free direction there should not act forces neither disturbances.

Therefore, the Drag Free controller has to compensate disturbances and maintain the cubes at the center of the cage without acting on them. The strategy adopted is to make the spacecraft follow the test masses.

The control of the vertical translation of the masses worths mentioning too. It is divided into two contributions: a common mode, due to solar pressure, and a differential mode. The first one is compensated through the micro-propulsion thrusters, the second one by the electrostatic suspensions.

All the controllers have been design through *H-infinity* approach, based on the loop shaping technique. The requirements are expressed as power spectral density distribution of the main jitter variables. These are the starting point to write the weighting functions needed for the design. Basically, the tool uses two weighting functions as guidelines to design the controller and achieve the desired loop shaping of the closed-loop functions. Technically, the first weighting function accounts for the reference tracking and disturbance rejections, while the second one for the robustness and noises attenuation. Moreover, to account for the command activity another weighting function can be added. In this particular case, due to the MIMO nature of the problem, the weighing functions will be matrices of weighting functions. They are the inputs to the *mixsyn* tool that solves an optimization problem.

The design phase was followed by a validation one to test the robustness of the controllers against the parametric uncertainties and the variation fo the disturbances. A Monte Carlo campaign was carried out obtaining satisfactory results both in terms of robust stability and performance.

Chapter 1

Description of a space based observatory

In this first chapter it is presented a schematic explanation of a space based gravitational wave observatory. The next european mission LISA and the heritage of LISA Pathfinder are taken as examples to catch the important informations needed for the controller design.[6][7]

1.1 System Description

1.1.1 System

A space based observatory aims to create a space interferometer to detect Gravitational Waves (GWs) by measuring the relative displacement between two masses left free to fall along their geodesic trajectories.

It consists of three spacecrafts (SCs) in a triangular constellation. The mean length is equal to 2.5 milion km and its center moves on an heliocentric orbit, located at $50 \cdot 10^6$ km up to $65 \cdot 10^6$ km distance from the Earth, fig. 1.1. Each spacecraft occupies one of the three vertices and the variation of the corresponding angle, between 59° and 61° , is referred to as *breathing angle*.

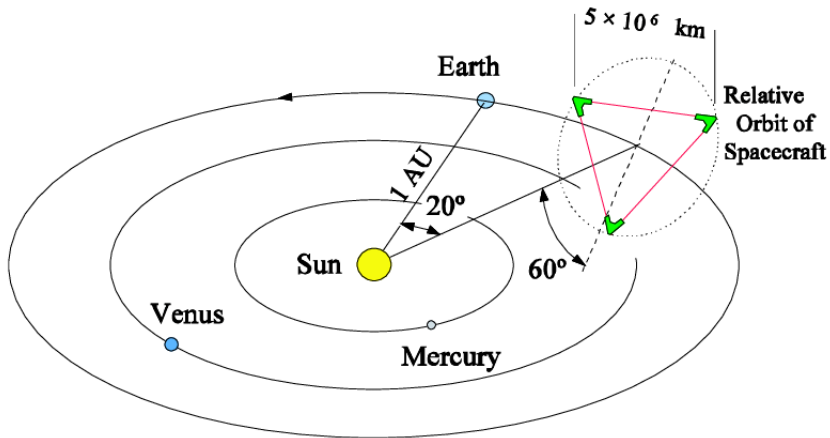


Figure 1.1: Spacecraft constellation.[1]

Each spacecraft consists of:

- a circular surface of solar array of 14 m^2 ;
- a science module;
- a propulsion module.

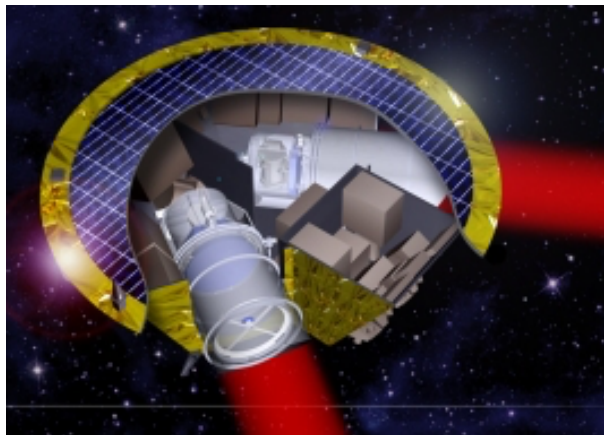


Figure 1.2: Cutaway view of LISA spacecraft.[2]

On the lateral surface of the science module, nine cold-gas actuators are displaced

in three pods at 120° apart from each other, creating the actuation system referred to as Micro-Propulsion Systems (MPS).

Moving inside the science module, it is mainly composed of two Optical Assemblies (OAs). It involves a telescope, an Optical Bench (OB), implementing the interferometers, and a Gravitational Reference Sensors (GRS), which is an advanced electrostatic suspension system, featuring a cage that hosts a test mass. The Gravitational Reference Sensors is an heritage of LISA Pathfinder [8].

The Optical Assemblies are mechanically linked to the spacecraft such that only the yaw rotation is allowed. The telescope has to ensure the laser link between the spacecrafts.

The TMs are gold-platinum cubes of 46mm side and 1.96 kg mass each.

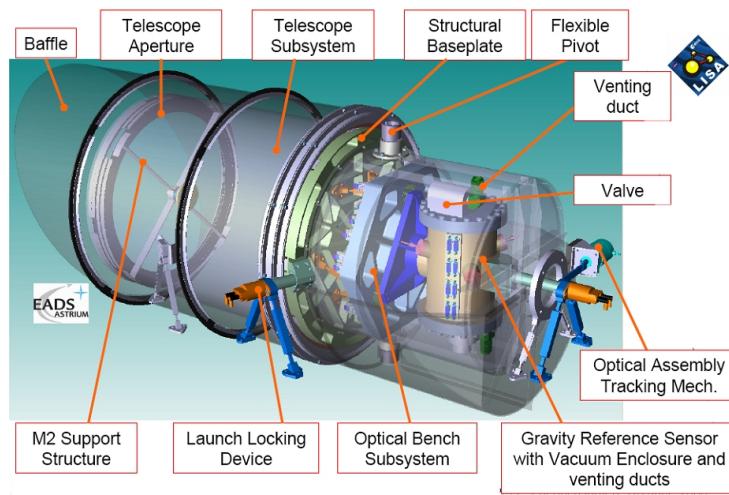


Figure 1.3: Lisa telescope.[3]

There are defined different local reference frames, deeply described in the next section. One of them is the Optical Assembly reference frame, whose x -direction is referred to as the *drag free direction*. As the name suggests, it is the direction along which the cubes have to be in drag free condition, i.e. without any external forces or disturbances to ensure that only Gravity acts on them.

However, although they should be suspended, the presence of local gravitational and electromagnetic field creates a coupling between them and the spacecraft.

Therefore, each SC-TMs system is composed of a spacecraft, free to move, two optical assemblies rotating around the z -axis, two cubes free to rotate and move

along all directions.

To summarize, the resulting Degrees of Freedom are:

- 3 DoFs for each Spacecraft Position, r_{SC}
- 3 DoFs for Spacecraft Attitude, θ_{SC}
- 6 DoFs for Test Masses Attitude, θ_{M1}, θ_{M2}
- 6 DoFs for Test Masses Position, r_{M1}, r_{M2}
- 2 DoF for the OAs, $\zeta_{1,2}$

They represent also the system's output, except for the spacecraft translation, involved in the test position, being expressed as the relative distance with respect to the spacecraft.

The available actuators depend on the mission phase considered. During the drag free phase, the inputs at the system are represented by:

- Micro-Propulsion thrusters, *MPS*: provide force and torque to steer the spacecraft;
- Electrostatic Suspension, *EF* and *EM*: provide forces and torques to act on the test masses, but in the science mode the x -force is off not to introduce too much noise;
- Optical Assembly motor: provides the torque to control the opening angle between the two optical assemblies;

For what concerns the sensing side, the output of the system are obtained through the following sensors:

- Differential Wavefront Sensors *DWS*: it is a functionality of the Optical Measurement System exploited during the drag free phase to obtain the spacecraft attitude θ_{SC} . It provides the azimuth and elevation angles of the SC with respect to laser beam coming from the other satellite. A second Differential Wavefront Sensor detects test masses pitch and yaw, $\theta_{TMi}(y, z)$ with respect to the optical reference frame

- Electrostatic Suspensions ES_{sens} : measures the test masses roll $\theta_{TM_i}(x)$ and the displacement r_{M_i} along yz -direction with respect to the cage frame
- the local Interferometer IFO : provides the the x -axis displacement

1.1.2 System Reference Frame

A schematic representation of the system and its main Reference Frames defined in [9] is presented below.

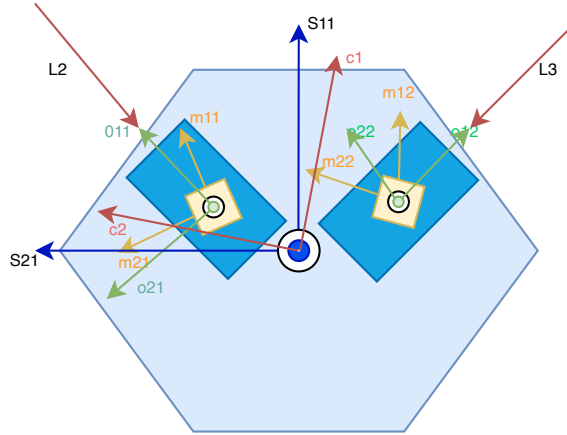


Figure 1.4: **SC and TMs Optical Assembly representation.**

The spacecrafts are referred to as SC_n , where $n = 1,2,3$, clockwise. The laser link between them is labelled with two sub-indices, from the spacecraft i to j .

The following reference frames can be defined, depicted in figure 1.4 and 1.1:

- the Sun-centered Inertial Reference Frame: $IRF = \{O_I, \mathbf{I}_1, \mathbf{I}_2, \mathbf{I}_3\}$;
- the Constellation Reference Frame, $CRF = \{O_c, \mathbf{c}_1, \mathbf{c}_2, \mathbf{c}_3\}$

It is relevant during the science mode, when the star tracker is not available and the SC attitude in IRF can not be known. The \mathbf{c}_1 axis is the bisetrix of the angle defined by the incoming laser, while \mathbf{c}_3 is perpendicular to the plane identified by \mathbf{L}_1 and \mathbf{L}_3 . The CRF is reconstructed on-board through the DWS sensors, which provides the azimuth and elevation angles of the

incoming laser wrt the optical reference frame. A deeper description of the algorithm is done in [9].

- *the Spacecraft Reference Frame* $SRF = \{O_S, \mathbf{s}_1, \mathbf{s}_2, \mathbf{s}_3\}$
- one *Optical Reference Frame* for each Test Mass $ORF_i = \{\mathbf{O}_{O_i}, \mathbf{o}_{1i}, \mathbf{o}_{2i}, \mathbf{o}_{3i}\}$ denoted with $i = 1$ for the left mass, the latter follows. O_{O_i} is at the center of the cage of each electrostatic suspension. Moreover, it holds $\mathbf{O}_{31} \parallel \mathbf{o}_{31} \parallel \mathbf{s}_3$ and \mathbf{o}_{1i} is parallel to the symmetry axis of the corresponding optical assembly

They are denoted as OAnm:

- n , denoting the spacecraft;
- $m = 1$, if the laser beam is transmitted clockwise;
- $m = 2$, counterclockwise;
- *the Test Masses Reference Frames*: $MRF_i = \{\mathbf{O}_{M_i}, \mathbf{m}_{1i}, \mathbf{m}_{2i}, \mathbf{m}_{3i}\}$, whose origin is centered at CoM of the referred mass and the axes are orthogonal to the TMs faces.

The TMs are labelled as:

- n , denoting the spacecraft;
- $p = 1$ or 2 , according to the considered optical assembly;

1.1.3 Dynamics Model: equations

In this section the nonlinear equations of the dynamics model reported in [9] are presented, with reference to ???. The whole plant is composed of 5 main subsystems. At first, the Newton-Euler's equations are written for each single subsystem, underlining the resulting coupling between them. Then, a linearization is performed.

Both command inputs and disturbances are considered as generic entries of the system.

SC rotation It is the Euler’s and kinematic equation for a single spacecraft. It describes the SC attitude with respect to the CRF.

The SC angular velocity can be expressed as:

$$\boldsymbol{\omega}_S = \boldsymbol{\omega}_{SI} - T_C^S \boldsymbol{\omega}_C \quad (1.1)$$

where $\boldsymbol{\omega}_S$ is the angular velocity wrt the constellation frame in SRF components, $\boldsymbol{\omega}_{SI}$ is its inertial angular velocity in SRF components and $\boldsymbol{\omega}_C$ in the constellation reference frame angular velocity. Its second derivative gives the acceleration wrt to CRF:

$$\dot{\boldsymbol{\omega}}_S = \dot{\boldsymbol{\omega}}_{SI} - \dot{T}_C^S \boldsymbol{\omega}_C - T_C^S \dot{\boldsymbol{\omega}}_C = \dot{\boldsymbol{\omega}}_{SI} + \dot{\boldsymbol{\omega}}_S \times T_C^S \boldsymbol{\omega}_C - T_C^S \dot{\boldsymbol{\omega}}_C \quad (1.2)$$

and $\dot{\boldsymbol{\omega}}_{SI}$ is derived from the Euler’s Equation:

$$\dot{\boldsymbol{\omega}}_{SI} = -J_S^{-1} \boldsymbol{\omega}_{SI} \times J_S \boldsymbol{\omega}_{SI} + J_S^{-1} \left(\mathbf{M}_T + \mathbf{D}_S - \sum_{i=1,2} (T_{Oj}^S I_{zz} \ddot{\boldsymbol{\zeta}}_j + T_{Oj}^S \mathbf{M}_{Ej} + \mathbf{b}_j \times \mathbf{T}_{Ol}^S \mathbf{F}_{El}) \right) \quad (1.3)$$

$$\dot{\mathbf{q}}_{SI} = \frac{1}{2} \mathbf{q}_{SI} \otimes \dot{\boldsymbol{\omega}}_{SI} \quad (1.4)$$

Where \mathbf{D}_s is the disturbances term, given by all the external torques acting on the spacecraft, \mathbf{M}_T is the total torque of thrusters. There are present also the reactions of the internal actuators, namely the optical assemblies and the electrostatic suspensions.

OA rotation It is reported a first approximation model describing the yaw dynamics:

$$\ddot{\boldsymbol{\zeta}} = -2\omega_N \dot{\boldsymbol{\zeta}}_j + -\omega_N^2 \boldsymbol{\zeta}_j + \frac{M_{OA}}{I_{zz}} - \frac{M_{Ej}}{I_{zz}} - T_S^{Oj} \dot{\boldsymbol{\omega}}_{SI} + \frac{D_{\zeta j}}{I_{zz}} \quad (1.5)$$

$$\omega_N = \sqrt{\frac{K_t}{I_{zz}}} \quad (1.6)$$

$$\xi = \frac{c_t}{2\sqrt{K_t I_{zz}}} \quad (1.7)$$

where ζ is the angle with respect to the rest direction. K_t , c_t and I_{zz} are respectively the stiffness, damping and inertia characteristics around the pivot axis. The command input is the torque provided by the OA motor, while M_E is the reaction torque of the electrostatic suspension.

TM rotation Now the Euler's and kinematic equations are applied to the test mass system, valid for both the cubes.

The angular velocity of each mass is:

$$\boldsymbol{\omega}_{Mj} = \boldsymbol{\omega}_{MIj} - T_{Oj}^{Mj} \boldsymbol{\omega}_{\gamma j} - T_S^{Mj} \boldsymbol{\omega}_{SI} \quad (1.8)$$

relative to the corresponding Optical Reference Frame but in the MRF components, explicitly considering both the contribution of the spacecraft and optical assembly angular velocity ω_S and ω_γ .

The angular acceleration will be the derivative:

$$\dot{\boldsymbol{\omega}}_M = \boldsymbol{\omega}_{MI} - \dot{T}_O^M \boldsymbol{\omega}_\gamma - T_O^M \dot{\boldsymbol{\omega}}_\gamma - \dot{T}_S^M \boldsymbol{\omega}_{SI} - T_S^M \dot{\boldsymbol{\omega}}_{SI} \quad (1.9)$$

where the inertial angular acceleration is given by the Euler's equation:

$$\dot{\boldsymbol{\omega}}_{MI} = -J_M^{-1} \boldsymbol{\omega}_{MI} \times J_M \boldsymbol{\omega}_{MI} + J_M^{-1} T_O^M (\boldsymbol{M}_E + \boldsymbol{D}_M + \boldsymbol{M}_{St}) \quad (1.10)$$

with \boldsymbol{M}_E is the Electrostatic Suspension torque, \boldsymbol{D}_M accounts for all the disturbances torque and $\boldsymbol{M}_{St} = S_{TR} \boldsymbol{r}_M + S_{RR} \boldsymbol{\theta}_M$ is the stiffness torque.

The TM attitude quaternion is:

$$\dot{\boldsymbol{q}}_M = \frac{1}{2} \boldsymbol{q}_M \otimes \boldsymbol{\omega}_{Mq} = \frac{1}{2} (\boldsymbol{q}_M) \boldsymbol{\omega}_{Mq} \quad (1.11)$$

TM and SC translation As said before, the TM translation is a consequence of the action of the drag free control, thus its dynamics depend on the TMs translation.

First, the Test Mass position relative to the cage center of the corresponding

optical assembly (ORF origin) in the IRF coordinate is:

$$\mathbf{r}_M^I = T_O^I \mathbf{r}_M \quad (1.12)$$

The acceleration is its second derivatives:

$$\ddot{\mathbf{r}}_M^I = T_O^I \Omega(\boldsymbol{\omega}_O) \mathbf{r}_M + 2T_O^I \boldsymbol{\omega}_O \times \dot{\mathbf{r}}_M + T_O^I \ddot{\mathbf{r}}_M \quad (1.13)$$

where $\boldsymbol{\omega}_O$ is the angular velocity of the optical assembly with respect to the IRF.

The test mass position can also be expressed as:

$$\mathbf{r}_M^I = \mathbf{r}_{MI} - \mathbf{r}_I - T_S^I \mathbf{b}_S - T_O^I \mathbf{b}_M \quad (1.14)$$

where it is explicit the position relative to the Spacecraft reference frame. In fact \mathbf{r}_{MI} is the distance wrt the IRF origin, \mathbf{r}_I between the SRF and the IRF origin, \mathbf{b}_S the distance between the pivot and the optical assembly, \mathbf{b}_M between the pivot and the cage center.

Performing the second derivative:

$$\ddot{\mathbf{r}}_M^I = \ddot{\mathbf{r}}_{MI}^I - \ddot{\mathbf{r}}_I - T_S^I \Omega(\boldsymbol{\omega}_{SI}) \mathbf{b}_S - T_O^I \Omega(\boldsymbol{\omega}_o) \mathbf{b}_M \quad (1.15)$$

where \mathbf{b}_S and \mathbf{b}_M are constant distances.

The inertial acceleration of the test masses and of the spacecraft are obtained by means of the Newton's Law:

$$\mathbf{r}_{MI}^{\ddot{}} = -\mu_{\odot} \frac{\mathbf{r}_{MI}}{|\mathbf{r}_{MI}|^3} + \mathbf{m}_M^{-1} T_O^I (\mathbf{F}_E + \mathbf{d}_M + \mathbf{F}_{St}) \quad (1.16)$$

$$\ddot{\mathbf{r}}_I = -\mu_{\odot} \frac{\mathbf{r}_I}{|\mathbf{r}_I|^3} + \mathbf{m}_s^{-1} \mathbf{T}_S^I (\mathbf{F}_T + \mathbf{d}_s) - \mathbf{m}_S^{-1} \sum_{i=1,2} \mathbf{T}_{Oj}^I \mathbf{F}_{Ej} \quad (1.17)$$

$\mathbf{F}_T + \mathbf{d}_s$ is the resultant of the thruster forces and external disturbances on the spacecraft. There are present also the Electrostatic Suspension contributions in the SC equation. While in the TMs equation the stiffness terms is given by $F_{St} = S_{TT} \mathbf{r}_M + S_{RT} \boldsymbol{\theta}_M$.

By combining the equation () and () the expression of the test masses acceleration

wrt the cage center in the IRF is:

$$\ddot{\mathbf{r}}_M^I = K_\Delta \Delta \mathbf{r}_{Ij} + m_M^{-1} T_O^I (\mathbf{F}_E + \mathbf{d}_M + \mathbf{F}_{St}) - m_S^{-1} T_S^I (\mathbf{F}_T + \mathbf{d}_S) + m_S^{-1} \sum_{i=1,2} T_{Oj}^I \mathbf{F}_{Ej} - T_S^I \boldsymbol{\Omega}_{SI} \mathbf{b}_S - T_{Oj}^I \boldsymbol{\Omega}_{Oj} \mathbf{b}_M \quad (1.18)$$

$K_\Delta \Delta \mathbf{r}_{Ij} \cong -\mu_\odot \frac{\mathbf{r}_I}{|\mathbf{r}_I|^3}$ represents the spacecraft/test masses gravity gradient.

SC-TM stiffness model One of the main enviromental disturbances is represented by the coupling between the Test Masses and the Spacecraft. It can be modelled as a system of virtual springs:

$$\begin{bmatrix} \mathbf{F}_{St} \\ \mathbf{M}_{St} \end{bmatrix} = \begin{bmatrix} S_{TT} & S_{RT} \\ S_{TR} & S_{RR} \end{bmatrix} \begin{bmatrix} \mathbf{r}_M \\ \boldsymbol{\theta}_M \end{bmatrix} \quad (1.19)$$

$S_{TT}, S_{RT}, S_{TR}, S_{RR} \in \mathbb{R}^{3 \times 3}$ are estimated stiffness matrices.

1.1.4 Linearization

The system described by the above equations results to be nonlinear and coupled. Although the nonlinear model is useful for simulation purpose, based on a reliable model, it is too complicated for being used during the design phase. For this reason, the system has been linearized, extrapolating the transfer function to be used in the controller design. The test masses/spacecraft attitude and the optical assemblies coordinates have been linearized around the target conditions, TMs translation around the center of the optical assembly cage:

$$\begin{aligned} \bar{\mathbf{r}}_{Mj} &= 0 \\ \bar{\boldsymbol{\theta}}_S &= 0 \\ \bar{\boldsymbol{\theta}}_{Mj} &= 0 \\ \bar{\mathbf{z}}_{OA} &= 0 \end{aligned}$$

A state-space model of the linearized equation can be written. The output vector is column of $n_y = 17$ and the input vector $n_u = 20$. During the Drag free phase the Electrostatic Suspension force along x is shut down, thus the input dimension is reduced to $n_u = 18$.

The resulting state, input and disturbance vector are:

$$\mathbf{x} = [\boldsymbol{\theta}_{SC}, \mathbf{r}_{M1}, \boldsymbol{\theta}_{M1}, \mathbf{r}_{M2}, \boldsymbol{\theta}_{M2}, \dot{\boldsymbol{\theta}}_{SC}, \zeta_1, \zeta_2, \boldsymbol{\omega}_{SC}, \mathbf{v}_{M1}, \boldsymbol{\omega}_{M1}, \mathbf{v}_{M2}, \boldsymbol{\omega}_{M2}, \boldsymbol{\omega}_{\zeta, M1}, \boldsymbol{\omega}_{\zeta, M2}] \in \mathbb{R}^{34 \times 1}$$

$$\mathbf{u} = [\mathbf{u}_T, \mathbf{u}_{EF1}, \mathbf{u}_{EM1}, \mathbf{u}_{EM2}, \mathbf{u}_{OA}] \in \mathbb{R}^{22 \times 1}$$

$$\mathbf{d} = [\mathbf{d}_S, \mathbf{D}_S, \mathbf{d}_{M1}, \mathbf{D}_{M1}, \mathbf{d}_{M2}, \mathbf{D}_{M2}, \mathbf{d}_G, \mathbf{u}_{OA}] \in \mathbb{R}^{28 \times 1}$$

$$\mathbf{y} = [\mathbf{r}_S, \boldsymbol{\theta}_S, \mathbf{r}_{M1}, \boldsymbol{\theta}_{M1}, \mathbf{r}_{M2}, \mathbf{r}_{M1}, \boldsymbol{\theta}_{M1}, \mathbf{r}_{M2}, \boldsymbol{\theta}_{M2}, z_{OA}] \in \mathbb{R}^{38 \times 1}$$

The linearized state equation is:

$$\dot{\mathbf{x}} = A\mathbf{x} + B\mathbf{u} + B^d\mathbf{d} \quad (1.20)$$

The inputs at the system are:

- Micro-Propulsion Assembly, for both forces and torques;
- Electrostatic Suspensions, for both forces and torques;
- Optical Assembly actuators.

Everything is summarized in the following table:

Variable	Symbol	Actuator	Sensor
Spacecraft Attitude	θ_{SC}	MPA (torque)	DWS_{SC}
Test Mass roll	θ_{TM_x}	ES (torque)	ES (sensing)
Test Mass pitch, yaw	$\theta_{TM_{y,z}}$	ES (torque)	DWS_{TM}
Test Mass drag free (x-axis)	r_{TM_x}	MPA (force)	ES (sensing)
Test Mass suspended coordinate (y,z-axis)	$r_{TM_{y,z}}$	ES (force)	DWS_{SC}

Table 1.1: Variables sum up.

Chapter 2

Actuators, Sensors and Disturbances

2.1 Actuators

In this section, only the actuators involved in the DFACS are presented, as shown in [10]

2.1.1 Micro Propulsion System

The Micro-Propulsion System is made of six cold-gas thrusters grouped in three pods at 120° on the lateral surface of the science module. They consist of two main parts:

- MTA (Micro Thruster Assembly)
- MPE (Micro Propulsion Electronics)

They are modelled as second order system that can provide desired forces and moments, obtained from the command input u_T coming from the controller. Each force can be considered composed by different contributions:

$$F_{T,real} = F_{T,theor} + F_{T,bias} + F_{T,noise} \quad (2.1)$$

The theoretical value is described by a second-order delayed dynamic model:

$$F_T = G_T * u_T(t - \delta_t)$$
$$G_T = \frac{\omega_T^2}{s^2 + 2\zeta_T \omega_T s + \omega_T^2}$$

The same holds for the torque M_T .

This expression accounts for the main characteristics of a dynamics model of an actuator, such as the actuation range, the delay, and more.

Analyzing it for the purpose of a controller design, the focus can be put only on the noise affecting the thrusters. It represents a noise entering the closed loop system, thus it should be filtered. It is modelled as a white noise w_d filter by a mask, whose transfer function is related to the considered direction of the force or torque. The filter masks have been obtained from the LPF literature.

They are summarized in the following table ??

2.1.2 Gravitational Reference Sensor

The LISA Pathfinder Mission was essential to check the functionalities and characteristic noises of the Gravitational Reference Sensor, which is one of the most relevant subsystem during the science phase.

It is an Electrostatic Suspension composed by 12 electrodes, 2 for each face of a cube, that controls and senses the TMs position and attitude, with respect to the center of the cage. The mathematical model considers:

- Measurement Range (WR mode and HR mode);
- Resolution (WR mode and HR mode);
- Sampling time;
- Noise.

As for the MPS, the noise can be modelled through a filtered white noise w_d . The filters are distinguished according to the mode and the working functionality. In the table 2.3, there are listed the noise shape filter for the actuation and high range mode.

Filter tf	Filter Mask
$H_{Txy} = \frac{1.3 \cdot 10^{-7} (s + 2\pi 1e-2)^2}{(s + 2\pi 1e-2 / ((50)^{0.5}))^2}$	<p style="text-align: center;">Bode Diagram</p>
$H_{Tz} = \frac{2.2 \cdot 10^{-7} (s + 2\pi 1e-2)^2}{(s + 2\pi 1e-2 / ((50)^{0.5}))^2}$	<p style="text-align: center;">Bode Diagram</p>

Table 2.1: MPS force noise filters.

2.2 Sensors

2.2.1 Optical Measurement System

The Optical Measurement System (OMS) is responsible to:

- generate the laser beam to be sent to the other SCs;

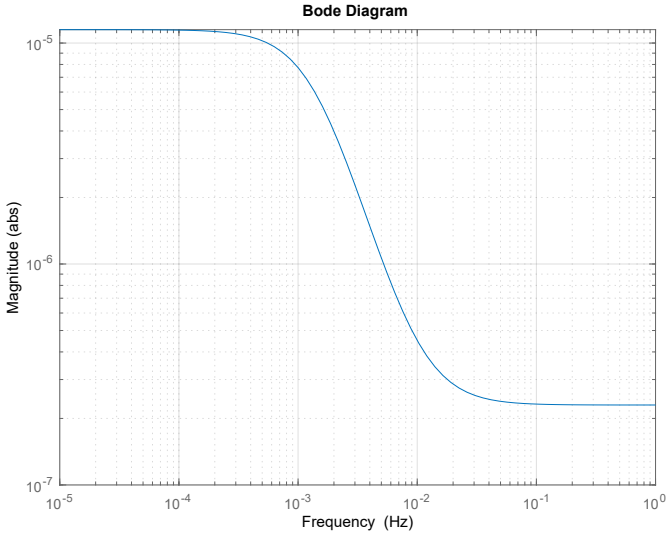
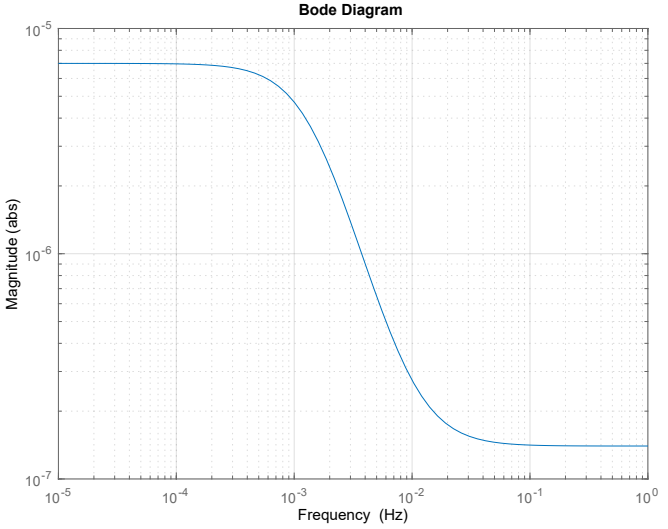
Filter tf	Filter Mask
$H_{Mxy} = \frac{2.3 \cdot 10^{-7} (s + 2\pi 1e-2)^2}{(s + 2\pi 1e-2 / ((50)^{0.5}))^2}$	
$H_{Mz} = \frac{1.4 \cdot 10^{-7} (s + 2\pi 1e-2)^2}{(s + 2\pi 1e-2 / ((50)^{0.5}))^2}$	

Table 2.2: MPS torque noise filters.

- do interferometry;
- measure distance along the sensitive axis;
- measure TMs pitch and yaw wrt the incoming laser beam.

It is composed by different subsystems, in particular the Optical Bench Interferometer and the telescope are interfaced through a small aperture of few mm. The

telescope also communicate with the other SCs, by sending and receiving the laser beam through an aperture. As said before the OMS provides also two entrances of the TMs attitude, thus it is also related with the electrode housing. In particular these angles are derived by the Differential Wavefront Sensing, heritage of LPF.

The sensor noise shape filters are:

The electrostatic suspension described in the previous subsection are characterized from the sensing point of view tab 2.5:

2.3 Disturbances

The disturbances that typically affect a system can be classified in four main classes:

- Environment;
- Actuation;
- Sensing;
- Parametric Uncertainties;

Although a real space observatory like LISA experiments much more disturbances, only the most relevant are described and modelled in this work. The LPF has been fundamental for testing the system and collect informations to draw the noise spectrum.

Environment The main environmental noises characterizing the LPF are:

- Electromagnetic Noise

It is caused by several sources as the on-board and interplanetary magnetic fields, since the TMs are electrical charged bodies they interact with them. Moreover, the high energy cosmic rays and solar particles can penetrate the spacecraft and charge the TMs.

- Thermal Noise

- Pressure Noise

The sources that contribute to this type of noise are mainly three. An acceleration noise is caused by the laser beam that interacts with the test masses, which reflects on them acting as a force. The second one is due to the Brownian motion of residual gas particles. Even though the masses and the GRS are hosted inside a vacuum chamber, some gas particles impact on the cubes causing one of the highest source of acceleration noise. The last one is the Solar Radiation which acts on the spacecraft.

- Self Gravity

It is a gravity attraction between the spacecraft and the test masses, which are attracted by the SC. It is composed of three components: a static gravitation field, gravitational fluctuations and gravity gradient (i.e. partial derivatives of the field wrt TMs DoFs). This last one creates a coupling between the TMs and the SCs that is modelled as a spring forces, whose coefficients have been estimated and involved in the SC-TM stiffness.

- Stiffness

It sums up different sources: magnetic, self gravity and electrical contribution.

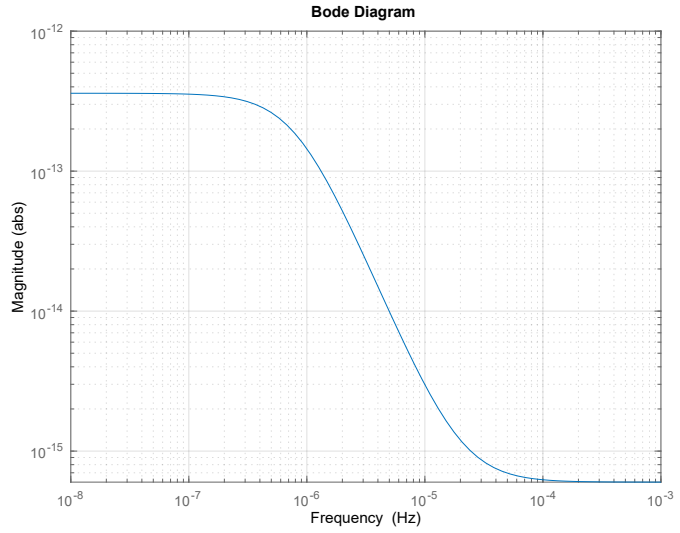
The following table collect the disturbances expression, other than actuator and sensor noises already presented.

Although a real system like LISA is affected by much more disturbances, the following table summarizes the most relevant used in this work, as first approximation:

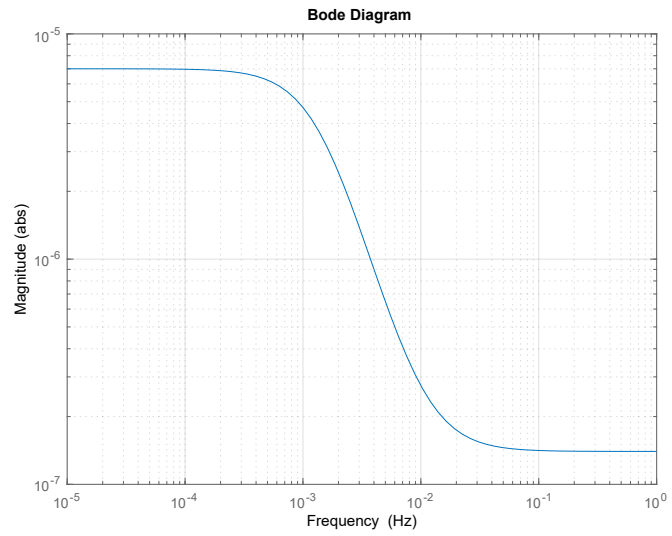
Filter tf

Filter Mask

$$EF_x = \frac{6 \cdot 10^{-16} (s + 4\pi 1e-5)^2}{(s + 4\pi 1e-5 / ((600)^{0.5}))^2}$$



$$EF_{yz} = \frac{5 \cdot 10^{-15} (s + 4\pi 1e-5)^2}{(s + 4\pi 1e-5 / ((2000)^{0.5}))^2}$$



$$EM_{xyz} = \frac{5 \cdot 10^{-17} (s + 4\pi 1e-5)^2}{(s + 4.5e-4 / ((2000)^{0.5}))^2}$$

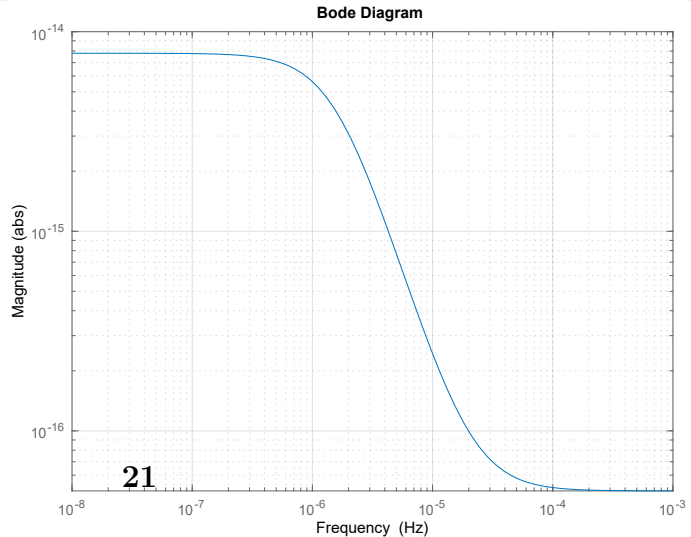
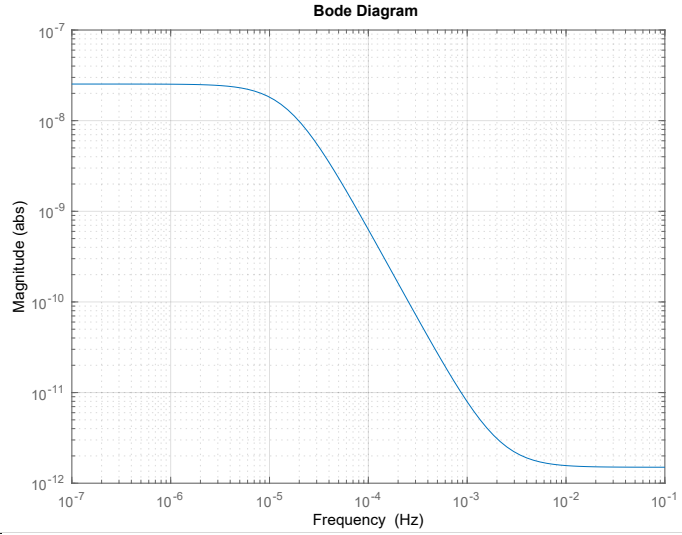


Table 2.3: ES ACTUATION noise filters.

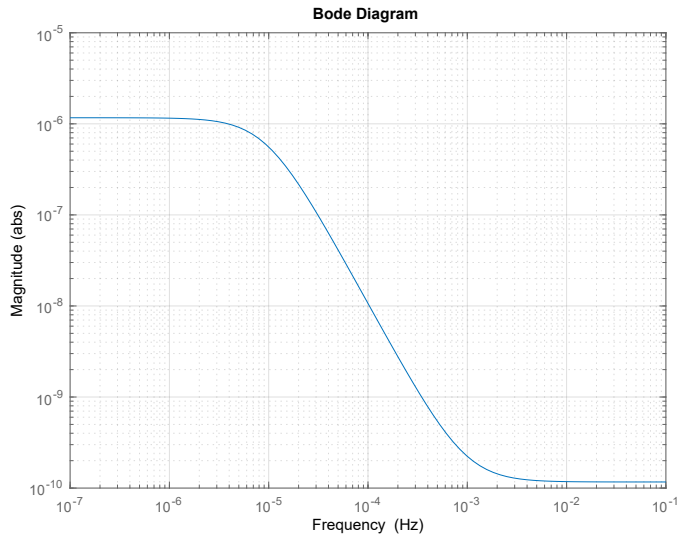
Filter tf

Filter Mask

$$H_{IFO, TM} = \frac{1.5 \cdot 10^{-12} (s + 1.3e-2)^2}{(s + 1e-4)^2} \frac{m}{\sqrt{Hz}}$$



$$H_{DWS, SC} = \frac{35 \cdot 10^{-9} (s + 6e-3)^2}{300 (s + 6e-5)^2} \frac{rad}{\sqrt{Hz}}$$



$$H_{DWS, TM} = \frac{5 \cdot 10^{-9} (s + 6e-3)^2}{(s + 6e-5)^2} \frac{rad}{\sqrt{Hz}}$$

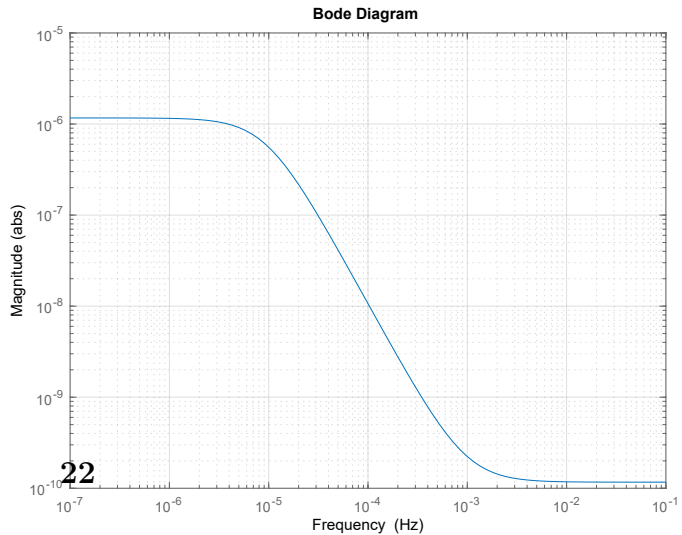
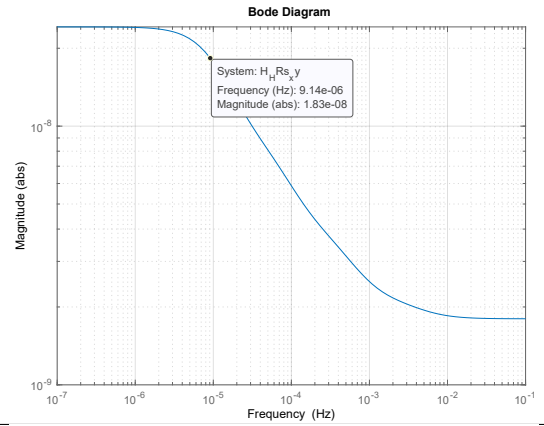


Table 2.4: OMS noise filters.

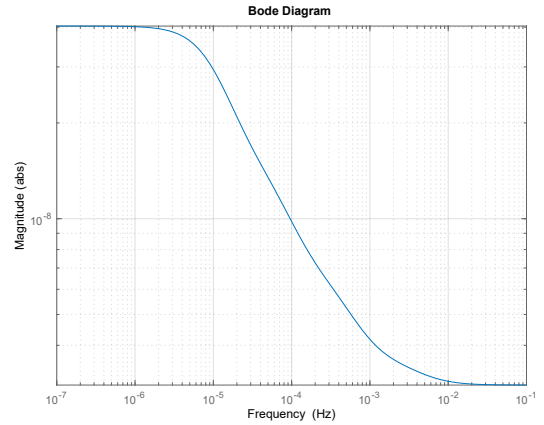
Filter tf

Filter Mask

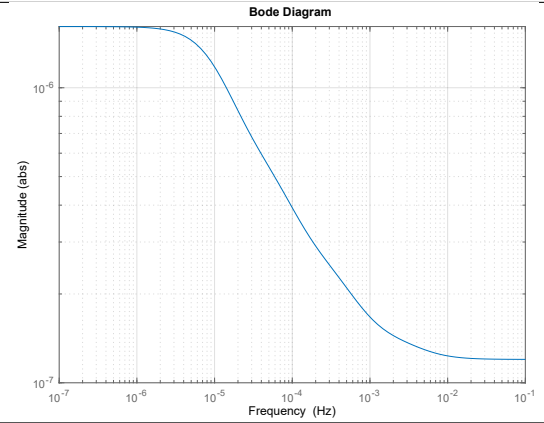
$$ES_{xy} = \frac{1.8 \cdot 10^{-9} (s+3e-2)(s+5.4e-3)(s+9.6e-4)(s+1.7e-4)}{(s+2.58e-2)(s+2.933e-3)(s+4.333e-4)(s+6e-5)}$$



$$ES_z = \frac{3 \cdot 10^{-9} (s+3e-2)(s+5.4e-3)(s+9.6e-4)(s+1.7e-4)}{(s+2.58e-2)(s+2.933e-3)(s+4.333e-4)(s+6e-5)}$$



$$ES_{tx} = \frac{2.7 \cdot 10^{-7} (s+3e-2)(s+5.4e-3)(s+9.6e-4)(s+1.7e-4)}{(s+2.58e-2)(s+2.933e-3)(s+4.333e-4)(s+6e-5)}$$



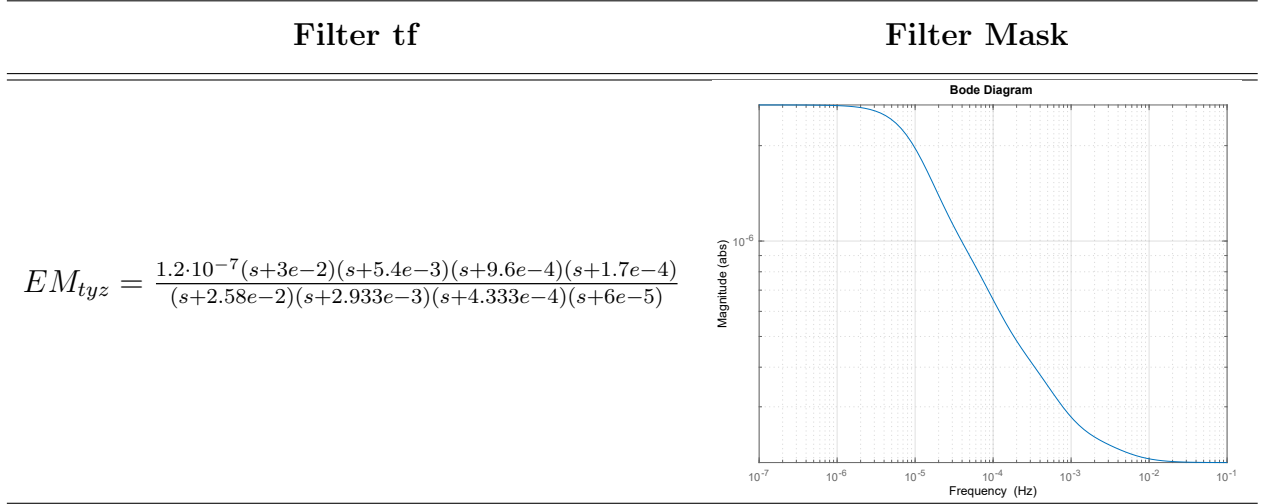


Table 2.5: Electrostatic Suspensions sensing noise filters.

Disturb	Symbol	Value
TM noise, force	H_{TMd}	$2 \cdot 10^{-15} \frac{(s+9e-3)(s+2.88e-3)(s+1.62e-3)(s+5.1e-5)}{(s+7.74e-3)(s+8.88e-4)(s+1.3e-4)(s+1.8e-5)} \frac{m/s^2}{\sqrt{Hz}}$
TM noise, torque	H_{TMD}	$9.2 \cdot 10^{-17} \frac{(s+9e-3)(s+2.88e-3)(s+1.62e-3)(s+5.1e-5)}{(s+7.74e-3)(s+8.88e-4)(s+1.3e-4)(s+1.8e-5)} \frac{rad/s^2}{\sqrt{Hz}}$
Solar Pressure Jitter	H_{SP}	$7.875 \cdot 10^{-11} \frac{(s+7.09e-2)(s^2+5.78e-3s+2.954e-4)}{(s+4.712e-3)(s^2+4e-3s+4e-4)} \frac{N}{\sqrt{Hz}}$

Table 2.6: OMS noise filters.

Chapter 3

Mixed Sensitivity Loop Shaping

The goal is to design a controller to stabilize the system and fulfilling the demanding requirements. The requirements are expressed in terms of the Power Spectral Density of the output vector and the linear acceleration along the drag free direction. Therefore, they have been translated in terms of the Laplace variable to make the design of the controller easier. Moreover, the actuator and sensor noises presented in the previous chapter have to be filtered to fulfill the requirements. In order to choose the control strategy the requirements and problem settings have been taken into account. Consequently, the Mixed Sensitivity Loop Shaping Approach, belonging to the H_∞ control design technique [11] [12], appeared to be a suitable choice. In this chapter it is presented the theoretical background that led to its choice.

3.1 Mixed Sensitivity Loop Shaping Approach

The *Mixed Sensitivity Loop Shaping Approach* [13] is a control design strategy derived from the *Loop Shaping Approach* [4]. The latter one looks for a controller by shaping the closed loop frequency response of a system. The main goals are:

- good reference tracking and disturbance rejection at low frequency;
- noise reduction and robustness at high frequency;
- manage the command effort.

3.1.1 Problem settings

The starting point is a general feedback control system:

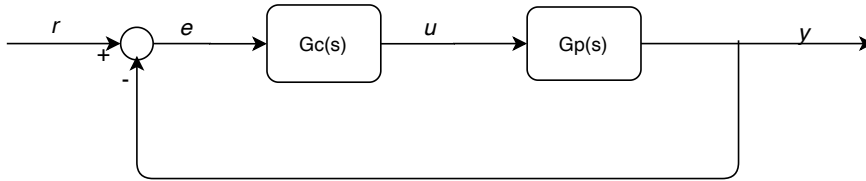


Figure 3.1: feedback control system.

Where:

- r : reference signal;
- e : error signal;
- u : input signal;
- y : output signal;

G_c is the controller, while G_p is the plant to control. The object is to make the output signal follow the reference. However, this is a non realist representation, because some important blocks are missed. In order to have a more reliable and realistic representation of a system, at least the following blocks have to be added:

- G_a : actuator block;
- G_s : sensor block;
- H_{act} : actuator noise;
- H_{sens} : sensor noise;
- H_{dist} : enviroment disturbs;

The goal of the control law can be re-formulated. It has to ensure good reference tracking, stability and *robustness*. This means that it has to stabilize the system and fulfill performances even in the prensence of disturbances and noises, but also parameter uncertainties. In the frequency domain, this leads to different constraints on the shape of the closed loop function.

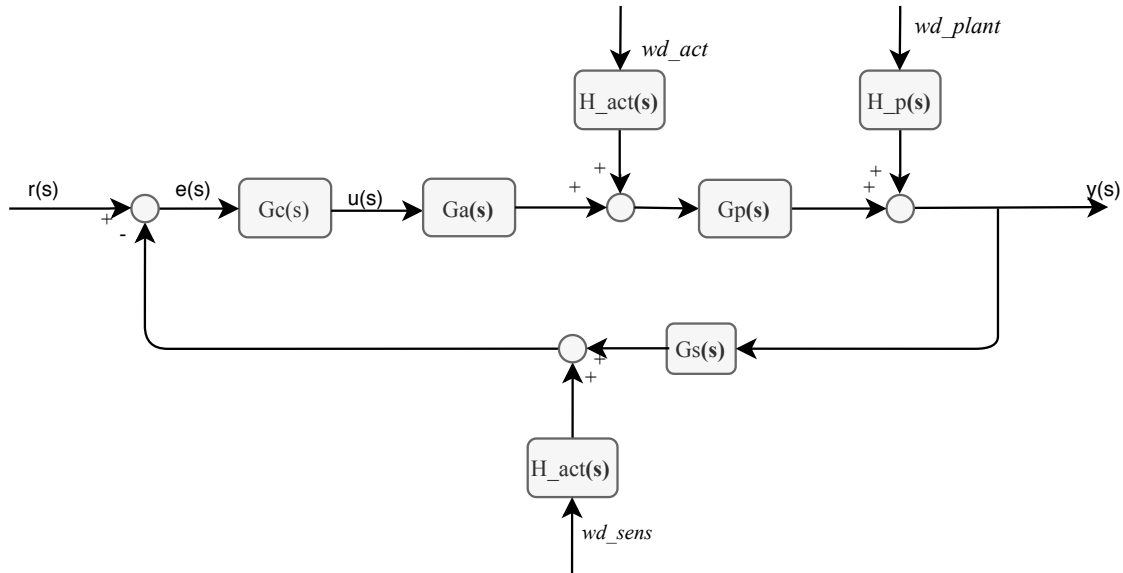


Figure 3.2: Feedback Control System.

3.1.2 Loop shaping approach

The *loop shaping approach* results to be a useful design strategy because it allows to find a trade off between two conflicting final objectives.

Basically, the idea is to maximize the open-loop gain to meet the performance specifications, but to make it drop below 0dB in the frequency region affected by measurement noise and poor model accuracy to avoid instability.

In particular, to reach a good reference tracking and disturbance rejection, the loop gain has to be high at low frequency, while it has to roll off at high frequency. In fact, at high frequency, the measurement noises and uncertainties of the model should be filtered not to enter the loop through the feedback.

The specifications for a general control problem are expressed in terms of *weighting functions*. Then these are used as guidelines to shape the desired open loop function L by the tool.

Starting from the considerations done before, two frequency regions can be identified. Consequently two corresponding weighting functions are defined.

The first one, labelled as W_1 accounts for the reference tracking and disturbance rejection. Thus it shapes the loop function at low frequency.

The other one, labelled as W_3 accounts for measurement noise and robustness, thus it shapes the loop function at high frequency.

A further function W_2 can be considered to limit the command activity.

The transition between these two areas can be set at the cross over frequency ω_c , where the loop function crosses the $0dB$ line.

The figure 3.3 shows graphically the final object to reach:

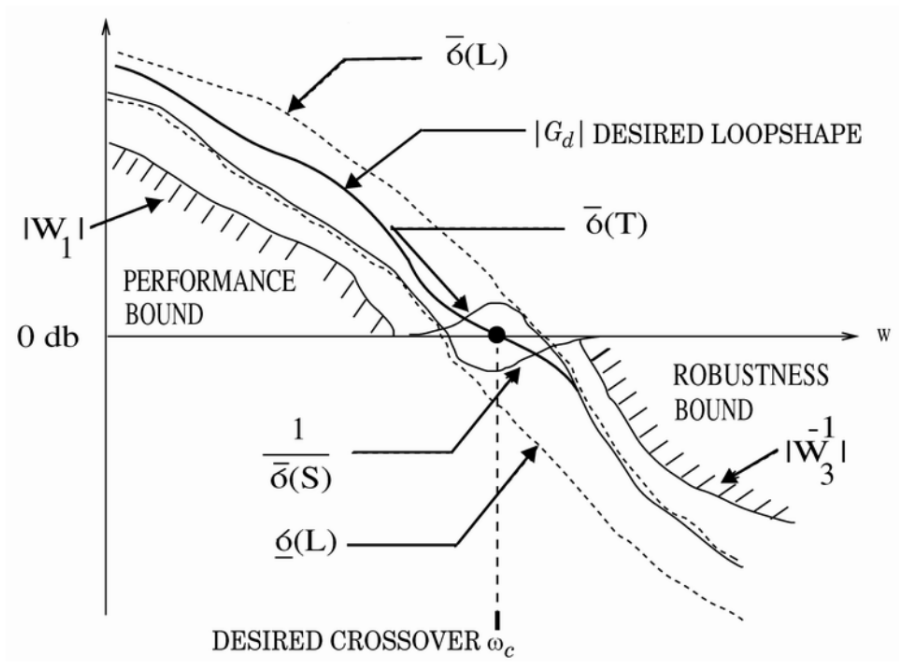


Figure 3.3: Loop shaping.[4]

The resulting design procedure can be synthesized in few steps:

- considerations about specifications and plant dynamics;
- derive and specify the desired loop shape;
- use *loopsyn* to compute the controller;
- analysis the frequency behaviuor of L ;
- check if the closed-loop response meets the specifications.

3.1.3 Mixed sensitivity loop shaping approach

The *mixed sensitivity* approach can be considered a step forward over the loop shaping approach. The working principle is the same, but the weighting functions can be derived through a more analytical reasoning.

The target is the same: find a controller with the best tradeoff between performance and robustness. These two requirements and the command effort are translated into three corresponding weighting functions W_i used by the tool *mixsyn* (mixed-synthesis) to compute the control law.

These functions are appended by the *mixsyn* to the starting feedback control system as shown in figure:

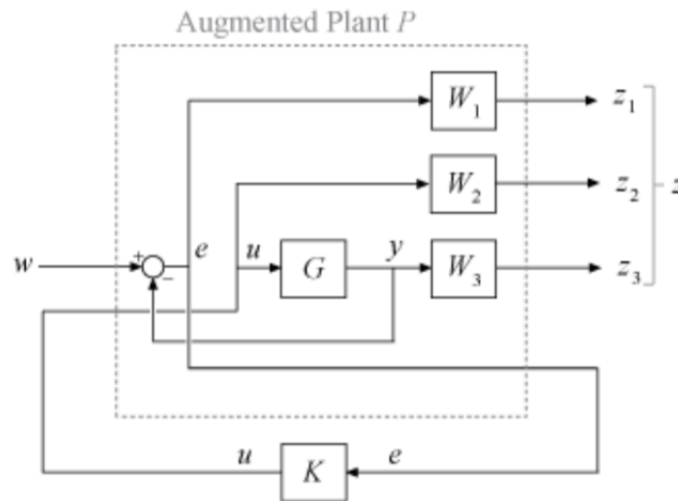


Figure 3.4: **Augmented Plant.**[5]

mixsyn seeks for a controller solving an optimization problem. It searches for the controller which minimizes the H_∞ norm of a given function, which is the transfer function of an augmented plant. It is obtained from the original by appending those weighting functions. The *augmented plant* P is shown in the figure:

The tool analyzes the new control system $[z; e] = P[w, u]$, with the weighting functions W_1, W_2, W_3 and with the new transfer functions $M(s)$ from the input w to

the new output z :

$$M(s) = \begin{vmatrix} W_1 S \\ W_2 G_c P \\ W_3 T \end{vmatrix} \quad (3.1)$$

The following functions can be defined:

- the *Sensitivity function* $S = (I + L)^{-1}$
- the *Complementary Sensitivity fcn* $T = I - S = L/(I + L)^{-1}$
- the *Control effort* KS

defined from the closed loop function $L = G_c \cdot P$. These functions are expression of the frequency response of the system and also the main parameters to tune, thus the name "mixed sensitivity".

The controller is computed as the one that minimizes the H_∞ norm of the transfer function $M(s)$ of the augmented plant, i.e. solving the problem:

$$G_c = \operatorname{argmin} \| M(s) \|_\infty \quad (3.2)$$

under some specific constraints.

3.1.4 Weighting Functions

It is clear from the problem setting that the choice of the weighting functions represents a fundamental step for a successful controller. In general for a good reference tracking, the closed loop L should have high gain at low frequency. On the other hand to have an attenuation of the measurement noises and robustness, L should roll off at high frequency. Looking at the expression of S and T , this means that the sensitivity function should be low at high frequency, while T small at high frequency.

This desired behaviour is translated in the shape of the weighting functions. In fact, considering the equation (2.1) and (2.2), the weighting functions are chosen to shape the sensitivity and complementary sensitivity functions. This can be derived

considering the H_∞ design constraints:

$$\| M(s) \|_\infty = \left\| \begin{array}{c} W_1 \\ W_2 G_c P \\ W_3 T \end{array} \right\|_\infty \leq 1 \quad (3.3)$$

equivalent to:

$$\| S(s) \|_\infty \leq |W_1^{-1}| \quad (3.4)$$

$$\| K S(s) \|_\infty \leq |W_2^{-1}| \quad (3.5)$$

$$\| T(s) \|_\infty \leq |W_3^{-1}| \quad (3.6)$$

Therefore, the reciprocal of the weighting function are designed as the desired shape for S and T .

As said before the weighting functions reflect two potentially conflicting objectives:

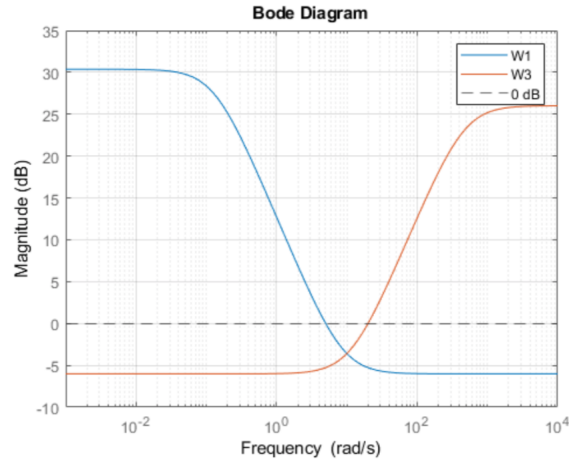
- W_1 : large in the control bandwidth to have a small S , to reach a good reference tracking and disturbance rejection;
- W_3 : large outside the control bandwidth for a small T , to ensure robustness and noise attenuation;
- W_2 : to act on the command activity, in particular to limit the control effort in a particular frequency range, its magnitude has to be increased.

This is graphically represented in the figure 3.5

Moreover, the function S and T are related to each other such that:

$$S + T = I$$

Therefore, *mixsyn* can not make both less than 0 dB in the same frequency range. When the weights are specified, W_1 and W_3 must be below the 0 dB in the frequency band where they cross each other.

Figure 3.5: **Weighting Functions.**

A further consideration regards W_1 . Being related to the sensitivity function, it likely has a pole in the origin, i.e. at $s = 0$. Although it would seem to be a good choice to reach zero steady state error, it also introduces an unstable pole at the system which can not be stabilized, making the optimization problem fail. It has to be replaced with a pole at low frequency, choosing $W_1 = \frac{1}{s+\delta}$, where $\delta = 0.000\omega_c$ or $0.00\omega_c$, and ω_c is the crossover frequency.

If a Single-Input Single-Output (SISO) system is considered, a single transfer function is used for the model and also the weighting functions result to be SISO. In case of Multi-Input Multi-Output (MIMO) system, the plant G is a matrix of N_u inputs and N_y outputs, $G \in \mathbb{R}^{[N_y, N_u]}$. Consequently, the weighting functions can be SISO function or square matrices of specific size, in particular W_1 a square matrix of N_y dimension, W_2 of N_u , W_3 of N_y .

The design procedure can be summarized in the following steps:

- analyze plant and performance specifications, which can be expressed in the time domain, for example in terms of the step response or steady-state error, or in the frequency domain as transfer functions;
- write the weighting functions from the consideration done in the previous step, i.e. the requirements have to be translated into suitable weighting functions;
- use *mixsyn* to design the controller, different options can be set for solving the

optimization problem;

- check the loop shape;
- verify the response in the time domain.

If the controller does not satisfy the required performances, a trial and error strategy has to be followed to choose more suitable W_i to reach the desired behaviour. For example, if the controller does not reach a good reference tracking, W_1 has to be modified.

A more practical approach about a possible procedure for writing the weighting functions is presented in the next chapter.

Chapter 4

Controller Design

The theoretical background of the previous chapter is the starting point for the next practical approach. In this chapter it is presented the procedure used in this thesis to design the control law, with particular mention of the weighting functions.

4.1 Problem setting

First of all, recall the feedback control system considered in this work. Focusing on the plant, it results to be a nonlinear and coupled system of 17 inputs, 20 outputs and 34 states for each SC-TMs system. The input vector is reduced to 18 entries because to the Electrostatic Suspension force along x is off.

However, looking at the table 1.1, some output variables are actuated by a single input system. For example, the Micro-Propulsion thrusters are involved only in the Spacecraft attitude control, or the Electrostatic Suspensions torque acts only on the TMs pitch and yaw. Therefore, the starting MIMO system can be splitted into MIMO subsystems. Although this entails multiple controllers, it has the advantage to simplify the design, also in terms of computational effort.

The Drag Free Attitude Control System (DFACS) involves the following controllers:

- $K_{att,sc}$: controls the spacecraft attitude through the MPS torque;
- $K_{att,TM}$: controls the test masses attitude through the EM torque;

- $K_{x, TM}$: controls the translation along x of the masses through the MPS forces (xy-axis);
- $K_{yz, TM}$: controls the test masses translation along the y axis and their relative translation along z through ES force;
- $K_{z, TM}$: controls the test masses common mode on z-axis due to the solar pressure through MPS force (z axis);
- K_{OA} : controls the optical assembly aperture;

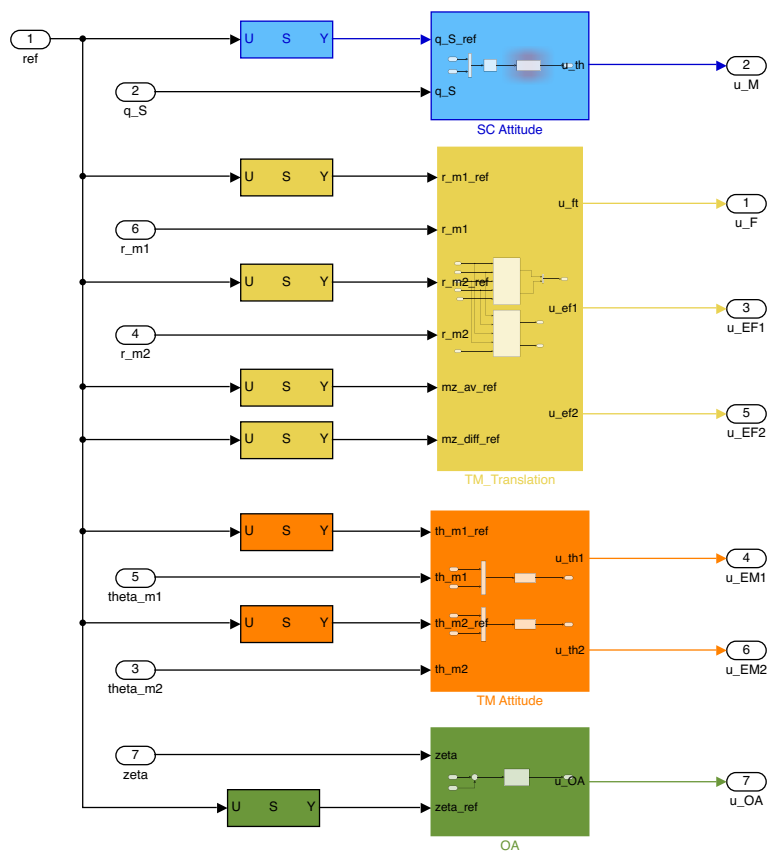


Figure 4.1: Control block.

The linearized equations presented in the first chapter have been used to derive the transfer functions of the plant, using a Simulink model previous developed in [14]. Through a Matlab script, the input-output transfer functions of the system

have been obtained, where the instruction *linmod* extrapolates the state-space linear model of the implemented block diagram. Then it can be easily translated in the s-domain. The script returns a matrix of transfer functions.

Moreover, the linearization has been done around two different operating points. In fact, the spacecraft mass and inertia change during the mission. Thus, it has been linearized at the begin and at the end of the cycle. The two different transfer function have been considered during the design phase of the spacecraft controller to write a more conservative weighting functions.

4.1.1 Performance Requirements

In this sections, the performance requirements are summarized. In [10], the mission objectives have been translated into a set of suitable requirements for the control subsystem. They have been consolidated through some considerations coming from the Lisa Pathfinder mission.

Two types of requirements are listed: functional and performance requirements. The former deals with the mission and system objectives, the latter with constraints for the controllers.

The DFACS Performace Requirements are presented here (Drag Free-Performance-IDnumber):

DF-P-010 Provides the frequency range where to verify the other requirements. There are defined a minimum range $f = [0.1mHz, 1Hz]$ and an ideal one $f = [0.01mHz, 1Hz]$. Both the intervals are consistent with the measurement bands of the science phase. Although the latter is more conservative, but it should be reach with a proper disturbance estimation and rejection.

DF-P-020 Provides an upper bound to the total acceleration noise jitter of the test mass along the single link TM to TM measurement. It is due to three different contributions: TM to SC, SC to SC and SC to TM, thus it takes into account several acceleration noise suorces, although they are not in charge of the DFACS.

$$REQ_{30} = 3 \cdot 1e - 15 \sqrt{1 + \left(\frac{0.4 \cdot 1e - 3}{fp}\right)^2} \sqrt{\left(1 + \frac{fp}{8 * 1e - 3}\right)^4} \quad (4.1)$$

DF-P-030 Limit the TM position jitter along the drag-free direction.

$$REQ_{30} = 2.5 \cdot 1e - 9 \cdot fp \quad (4.2)$$

DF-P-040 Limit the TM position jitter along the suspended coordinates

$$REQ_{40} = 5 \cdot 1e - 9 \cdot fp \quad (4.3)$$

DF-P-050 limit the TMs angular jitter for pitch and yaw of the test masses.

$$REQ_{50} = 10 \cdot 1e - 9 \sqrt{\left(1 + \frac{3e - 3}{fp}\right)^4} \quad (4.4)$$

DF-P-060 limit the Spacecraft position jitter.

$$REQ_{60} = 5 \cdot 1e - 9 \cdot fp \quad (4.5)$$

DF-P-070 bounds the spacecraft pointing accuracy

$$REQ_{70} = 10 \cdot 1e - 9 \quad (4.6)$$

DF-P-080 bounds on the spacecraft attitude jitter.

$$REQ_{80} = 10 \cdot 1e - 9 \cdot \sqrt{\left(1 + \frac{3e - 3}{fp}\right)^4}; \quad (4.7)$$

4.1.2 Weighting functions choice

The weighting functions represent the design parameters of the mixed sensitivity design approach, their suitable choice leads to the desired behaviour. They have been derived following the analytical approach designed in [14]. Looking at the design procedure outlined in the previous chapter, the first step is the analysis of the plant dynamics and performance specifications.

Plant Consideration Recalling the equation 3.1.4, the weighting functions are the inverse of the sensitivity and complementary sensitivity functions. Thus, they

are expression of the loop function L , which involves the plant transfer function. These last ones are the entries of the matrix derived from the linearization process described before.

Each row of the matrix contains the transfer functions of a single output wrt all the inputs. Although the linearization, due to the couplings affecting the system, the dynamics of a single variable depends also on the inputs not involved in its control. This means that the entries of the matrix corresponding to the other inputs are not zero. In practice, this does not represent a relevant problem, because their order of magnitude is much lower than the main inputs, thus they can be neglected. This important consideration reliably adheres to the constraints on the dimension of the weighting function, W_1 square matrix of N_y dimension and W_3 of N_u .

Performance Consideration The performance requirements are expressed as an upper bounds on the controllable variable in the frequency domain. Graphically, it means that its power spectral density plot has to be lower than Bode diagram of the amplitude of the corresponding REQ_i .

Therefore, they represent the starting point to derive the weighting functions.

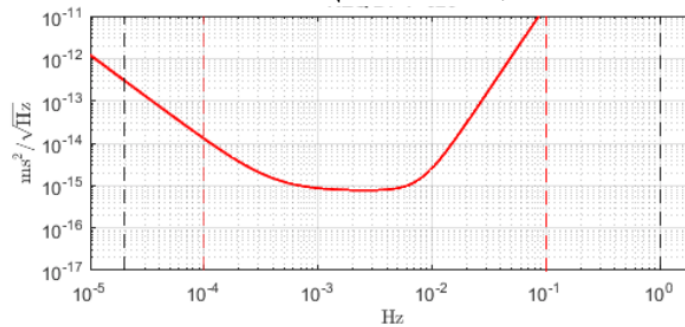


Figure 4.2: **Requirement example.**

The weighting functions are obtained from the combination of these two constraints.

In order to derive their expression, the block diagram representing the real control system and the augmented plant have to be compared.

First, recall the augmented plant:

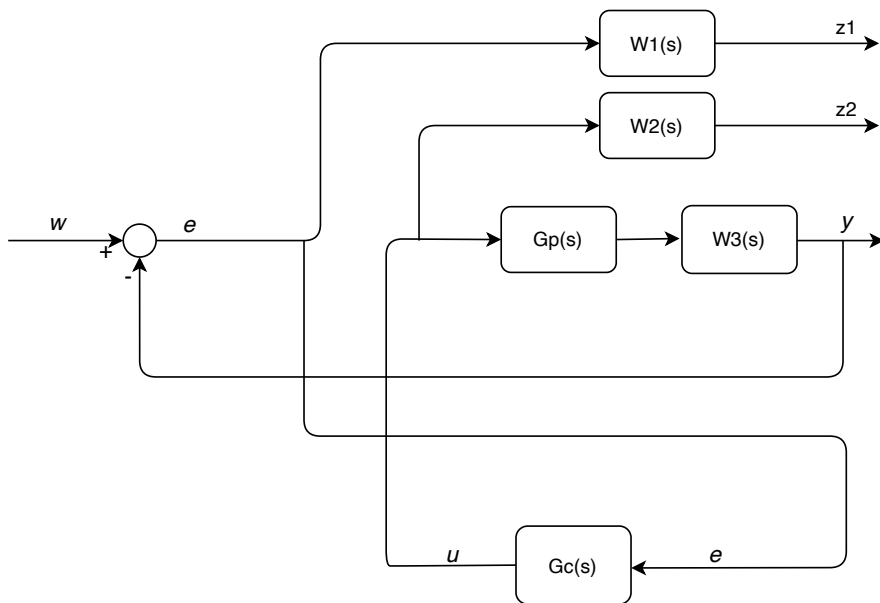


Figure 4.3: **Augmented Plant.**

and feedback control system of LISA, schematically represented in the Figure 4.4

The jitter variation of the output \tilde{y} has to be minimized with respect to the disturbances and noises and it has to be less than REQ_i .

First, the transfer function between the output and each input of the system are written. Then they are set lower than REQ_i .

The generic transfer function between the output and one of the inputs will be indicated as:

$$H_i = w_i \rightarrow \tilde{y} \quad (4.8)$$

For each noise or disturbance entering the plant, it is written the corresponding transfer function H_i . They are considered once at a time, shutting down the others. For example, considering only the actuator noise, turning off the environment

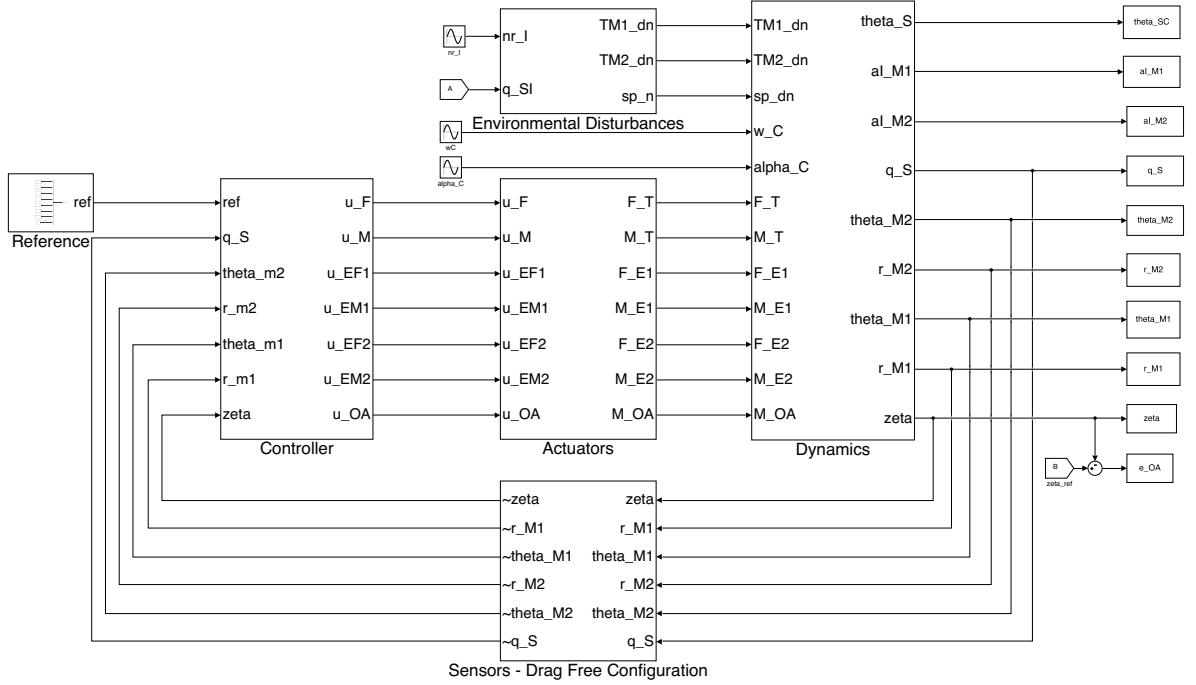


Figure 4.4: Feedback control system of the GWs observatory.

disturbances and sensors noise, it results:

$$H_{1,1}(s) = w_{act} \rightarrow \tilde{y} \quad (4.9)$$

and from the block diagram algebra:

$$H_{1,1}(s) = \frac{H_{act}(s)G_p(s)}{1 + G_c(s)G_p(s)G_s(s)G_a(s)} \quad (4.10)$$

If the disturbance affecting the plant is considered:

$$H_{1,2}(s) = w_{plant} \rightarrow \tilde{y} \quad (4.11)$$

and

$$H_{1,2}(s) = \frac{H_{plant}(s)}{1 + G_c(s)G_p(s)G_s(s)G_a(s)} \quad (4.12)$$

The second constraint comes from the transfer function between \tilde{y} and sensor noise, turning off the other inputs of the system:

$$H_2(s) = w_{sens} \rightarrow \tilde{y} \quad (4.13)$$

where

$$H_2(s) = \frac{H_{sens}(s)G_p(s)G_c(s)}{1 + G_c(s)G_p(s)G_s(s)G_a(s)} \quad (4.14)$$

The same constraint REQ_i applies for all H_i of the same variable, in the frequency range specified by *DF-P-010*:

$$|H_{1,1}(j\omega)| \leq |REQ(j\omega)| \quad \forall \omega : 2e^{-5}Hz \leq \omega \leq 1Hz \quad (4.15)$$

$$|H_{1,2}(j\omega)| \leq |REQ(j\omega)| \quad \forall \omega : 2e^{-5}Hz \leq \omega \leq 1Hz \quad (4.16)$$

$$|H_2(j\omega)| \leq |REQ(j\omega)| \quad \forall \omega : 2e^{-5}Hz \leq \omega \leq 1Hz \quad (4.17)$$

The expressions of H_i derived before can be substituted:

$$\left| \frac{H_{act}(s)G_p(s)}{1 + G_c(s)G_p(s)G_s(s)G_a(s)} \right| \leq |REQ(j\omega)| \quad (4.18)$$

$$\left| \frac{H_{plant}(s)}{1 + G_c(s)G_p(s)G_s(s)G_a(s)} \right| \leq |REQ(j\omega)| \quad (4.19)$$

$$\left| \frac{H_{sens}(s)G_p(s)G_c(s)}{1 + G_c(s)G_p(s)G_s(s)G_a(s)} \right| \leq |REQ(j\omega)| \quad (4.20)$$

recalling that:

$$\begin{aligned} L &= G_s(s)G_a(s)G_p(s)G_c(s) \\ S &= \frac{1}{1+L} \\ T &= \frac{L}{1+L} \end{aligned}$$

it results:

$$|H_{act}(s)S(s)Gp(s)| \leq |REQ(s)| \quad (4.21)$$

$$|H_{plant}(s)S(s)| \leq |REQ(s)| \quad (4.22)$$

$$|H_{sens}(s)T(s)| \leq |REQ(s)| \quad (4.23)$$

$$|S(s)| \leq \left| \frac{REQ(s)}{H_{act}(s)Gp(s)} \right| \quad (4.24)$$

$$|T(s)| \leq \left| \frac{REQ(s)}{H_{sens}(s)} \right| \quad (4.25)$$

Comparing these equations with the theoretical expressions derived in the previous chapter, two constraints are obtained on the Sensitivity function, one on the Complementary sensitivity functions. Thus there are two constraints on W_1 and one on W_2 .

W_1 can be written choosing the constraint that leads to a lower value of the sensitivity dcgain. Otherwise, the actuators noises results to be higher than the plant disturbances, thus the weighting functions can be written considering it. However, to be more conservative, all the noises and disturbances influencing the sensitivity function have been sum and considered as a whole.

The final weighting functions are:

$$W_1(s) = \frac{(H_{act} + H_{plant})(s)Gp(s)}{REQ(s)} \quad (4.26)$$

$$W_3(s) = \frac{H_{sens}(s)}{REQ(s)} \quad (4.27)$$

The weighting function W_2 accounts for the command effort. At first instance, it can be chosen as a constant value to limit the command activity, for example,

not to exceed actuators saturation. Actually, when a trial and error procedure is performed, by adjusting the weighing functions to achieve best performances, its value influences the result. An higher value limits the command activity, means that the loop gain at low frequency will be lower. At the same time it also limits the controller dynamics, leading to a more smooth transfer function. Thus, it can be used as tunable parameter to act on the controller, even though it does not have a specific analytic expression.

The optimization problem that *mixsyn* solves results to be:

$$G_c = \operatorname{argmin} \| M(s)_{w \rightarrow z} \|_{\infty} \quad (4.28)$$

subject to:

$$|S(j\omega)| \leq \left| \frac{1}{W_1(j\omega)} \right| = \left| \frac{REQ(j\omega)}{H_{act}(j\omega)G_p(j\omega)} \right| \quad (4.29)$$

$$|T(j\omega)| \leq \left| \frac{1}{W_3(j\omega)} \right| = \left| \frac{REQ(j\omega)}{H_{sens}(j\omega)} \right| \quad (4.30)$$

$$|K(j\omega)| \leq \left| \frac{1}{W_2(j\omega)} \right| = N \quad (4.31)$$

where the augmented model is:

$$M(s)_{w \rightarrow z} = \begin{bmatrix} W_1 S \\ W_2 G_c G_p \\ W_3 T \end{bmatrix} \quad (4.32)$$

In Matlab, the resulting set for it is:

```
opts = hinfynOptions('Method','LMI','Autoscale','on','Display','on')
[K,gamma,CL]= mixsyn(P,W1*N1,W2*N2,W3*N3,opts)
```

The above Matlab command can be read as: *mixsyn* computes the controller K which minimizes the H_{∞} norm of the augmented plant obtained by appending the weighing function W_i to the plant.

Each one of the weighing functions can be multiplied by a coefficient N_i . It can be useful in a trial and error procedure to achieve better performances, but also to move the crossing point between W_1 and W_3 below 0 db, when this does not happen.

W_1 and W_3 are square matrices respectively of N_y and N_u dimension. In fact, an important observation is that the variables of same MIMO subsystem are subject to different noises, thus the entries of the matrix are different.

Although this does not apply for the reported example, looking at the table 4.6, the test masses attitude is an explicative example. The roll rate is sensed and controlled through different instruments than the pitch and yaw. The resulting weighting functions are different. The chance to draw ad hoc the weighting function with different noises, while designing a single control law, represents one of the strenghts of this approach.

Moreover, through "*hinsynOptions*" it is possible to choose different options for the computation.

It has been set:

- 'Method': it is possible to choose between three different optimization algorithm:
 - 'RIC': Riccati-based, it is the default and also the fastest. However, it can handle singular problem only adding extra disturbances and erros. This is called regularization problem and is atumatically done by mixsyn;
 - 'LMI': Linear Matrix Inequalites, it is computationally intensive, but does not require any additional options;
 - 'MAXE':Maximum entropy.

Being the constraints expressed as inequalities, the 'LMI' has been chosen.

- 'Autoscale': automatically scale the plant states, controls and measurements, to improve the numerical accuracy, but the returned controller K is in the original unscaled coordinates.
- 'Display' on shows the progressing steps of the algorithm in the command window. For the LMI alghoritm shows the best γ achieved at each iteration, being $\gamma = \| M(s) \|_\infty$.

This represents the starting set up for the controller design. As said before, the first iteration can be done without any restrinction on W_2 , declared as an empty

vector, but this would probably lead to a saturation in simulation. Thus its value has to be increased.

Once the control law has been obtained, the first check can be done graphically. The Bode diagram of the magnitude of the functions H_1 and H_2 are plotted, and the inequalities 4.1.2 and 4.1.2 are checked. If the bound is crossed, the starting weighting functions have to be modified. More details about the implementation of this procedure is provided in the next section.

In the following table are listed the MIMO subsystems and the corresponding matrices of weighting function:

4.1.3 Example: Drag free control design

In this section it is presented the design of the Drag Free controller, i.e. the controller along the x direction, also called *sensitive direction*, for both the test masses. Remember that is the direction where the data for science purpose are collected, thus it must respect the requirements not to invalidate the experiment.

It is the most interesting system, because the aim of the controller is to maintain the test masses at the center of the cage by adjusting the spacecraft position to follow them. In practice, this means that the DF-controller receives as input the position error of both test masses along x and sends the command input u at the Micro-Propulsion system which provides thrust in terms of the x and y component of the forces.

The Figure 4.5 shows an abstract of the simulink system, compared with a schematic representation 4.6:

The noises affecting the test masses translation along x are:

- $H_{MPS,xy}$: actuator noise on the Micro-Propulsion thrusters;
- H_{IFO} : measurement noise of the IFO sensor;

The environment disturbances are:

- H_{SP} : Solar pressure acting on the spacecraft, to be compensated by the micro-thruster;
- H_{TMd} : Brownian motion of the residual particles;

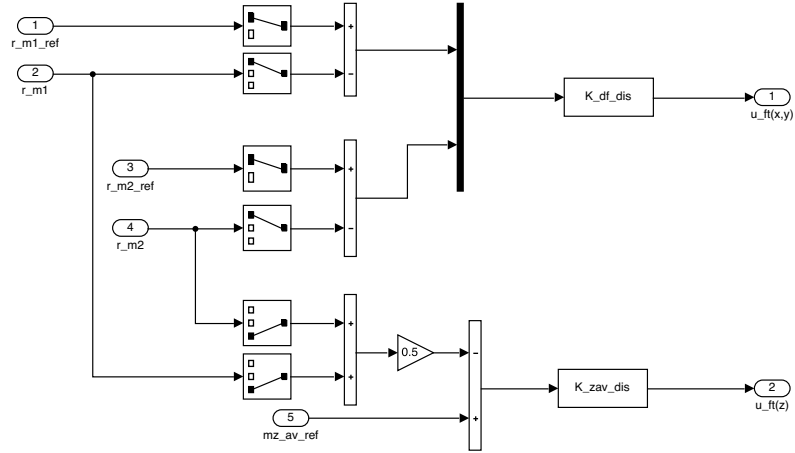


Figure 4.5: Simulink model.

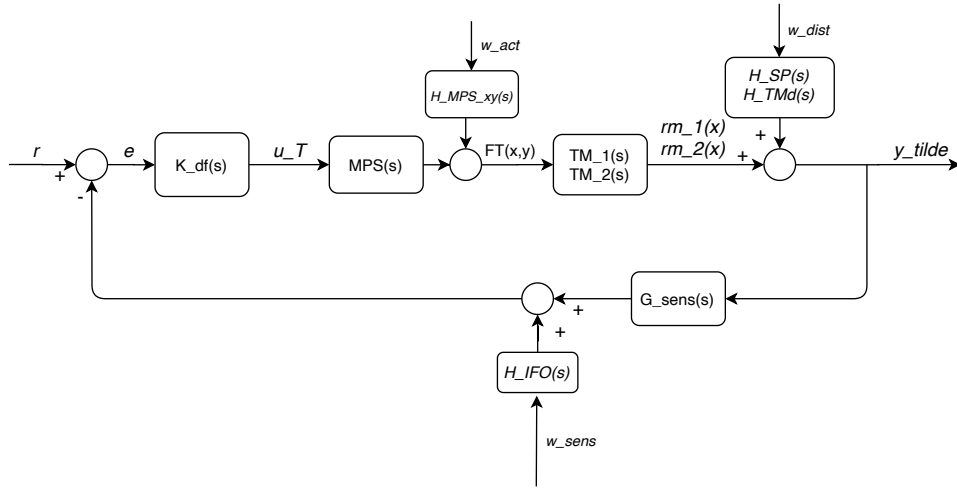


Figure 4.6: Block scheme.

The disturbances acting on the plant, i.e. H_{SP} and H_{TMd} , and the actuators noise have effects on the sensitivity function, then they are involved into W_1 . The measurement noise on reflects in W_2 . As demonstrated in the first section. The requirement REQ_{40} sets the upper bound on x translation jitter.

The resulting weighting functions are:

$$[W_1] = \begin{bmatrix} \frac{(H_{SP}+H_{TMd}+H_{nMPS_{xy}})P(1,1)}{B_{40}} & \frac{(H_{SP}+H_{TMd}+H_{MPS_{xy}})P(1,2)}{B_{40}} \\ \frac{(H_{SP}+H_{TMd}+H_{nMPS_{xy}})P(2,1)}{B_{40}} & \frac{(H_{SP}+H_{TMd}+H_{MPS_{xy}})P(2,2)}{B_{40}} \end{bmatrix} \quad (4.33)$$

$$[W_3] = \begin{bmatrix} \frac{H_{IFO}}{B_{40}} & 0 \\ 0 & \frac{H_{IFO}}{B_{40}} \end{bmatrix} \quad (4.34)$$

The plant transfer function P introduces a pole of multiplicity 2 at $s = 0$ in W_1 , making it unstable. This can not be handled by the tool. Therefore, It has to be replaced with a pole at low frequency, small compared to the dynamics of the system, but not too much to avoid numerical inaccuracy. It can be set as $\delta = 0.001 \cdot \omega_c$ or $\delta = 0.0001 \cdot \omega_c$. Where ω_c is the crossing frequency between (W_1, W_2) . This is just a reference range, where to vary the low frequency pole focusing the consequences on the obtained control law. In fact, a lower value of δ could lead to a reduction of the dcgain of the controller, thus of the loop function. Even though this avoids the amplification of the noise introduced by the sensors in the feedback control system, it also reduce the disturbances rejection.

At first instance, the design can be done without any rescription on W_2 .

Before testing the controller in the simulation enviroment, it is graphically checked if the constraints on the upper bound (equation 3.12 e 3.13) are satisfied, figure 4.7

This kind of check provides an important first sight on the performances. In fact, due the high noise affecting the measurements, the requirement could result unfeasible at a certain frequency, as demonstrated in technical note [14]. For example, the drag free requirement is unfeasible at frequencies lower than $5 \cdot 10^{-5}$.

Although the function may respect the limit, when testing the controller in the complete simulink enviroment it may happens that the requirements are not perfectly met or more likely the actutors saturate. Consequently, the value of W_2 has to be increased. Then the new controller is tested. At this point a trial and error procedure follows to achieve the best performances, by changing the coefficients N_i and W_2 . In this way the "weight" associated to the referred function changes, while affecting the loop shape.

In fact, another possible check on frequency behaviour of the system is done

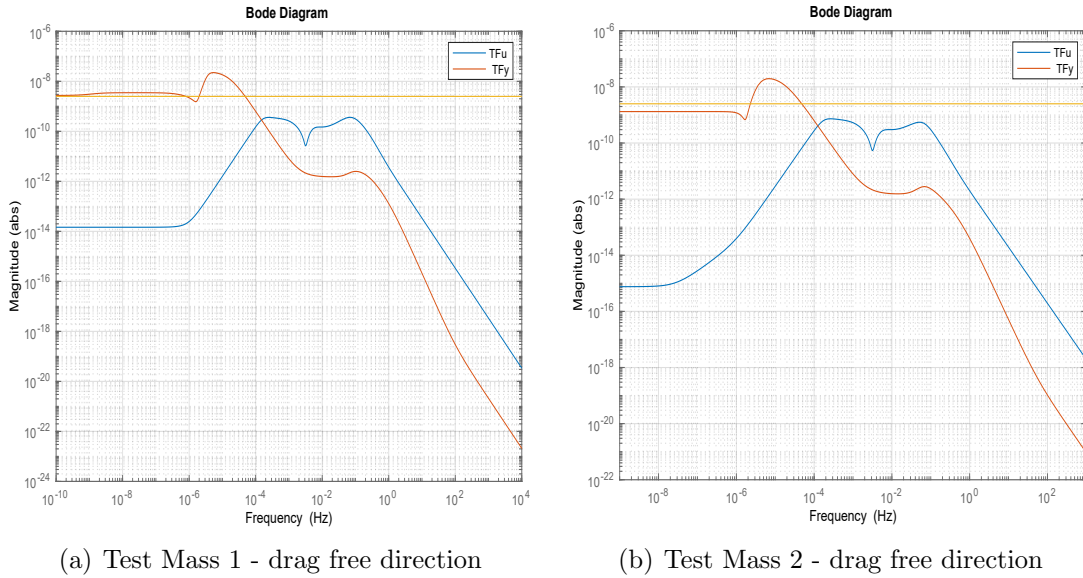


Figure 4.7: Sensitivity and Complementary Sensitivity functions.

on the loop shapes as in the loop shaping approach. Remembering the qualitative behaviour shown in the figure 3.3, also in this case frequency response of the loop can be checked. It is shown in the figure the frequency at which it is unfeasible.

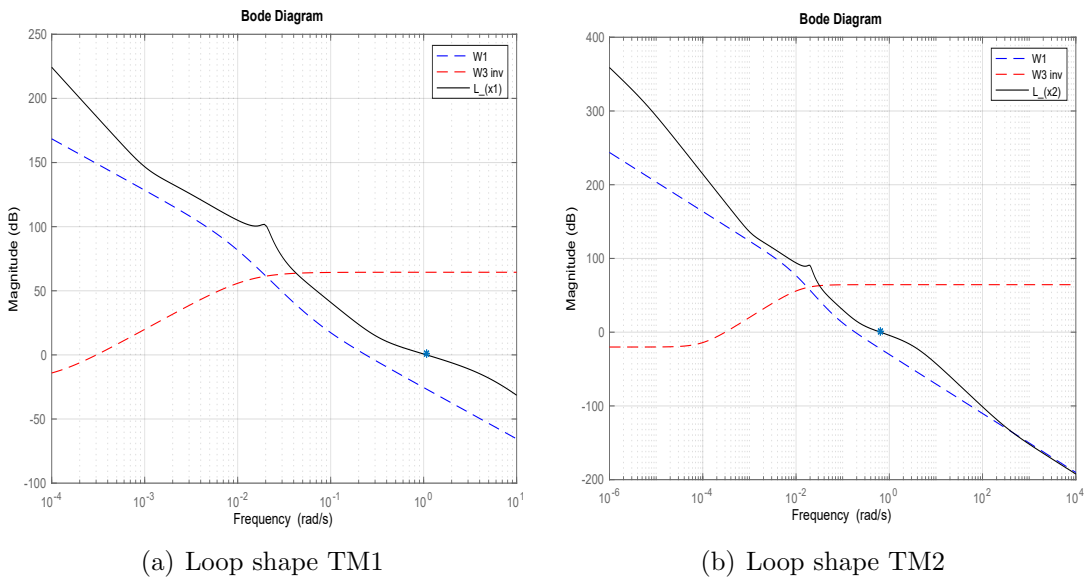


Figure 4.8: Drag free loop shape.

Once the control law has been obtained, the next important step is its order reduction. In fact, due to the high order of the weighting functions and the coupling plant, the order of the controller returned by *mixsyn* is high. It has poles and zeros at very high or low frequencies with respect to the bandwidth of the system. Therefore they can be deleted because they do not influence the system dynamics.

4.1.4 Controller Simplification

The goal is the reduction of the controller order while preserving its important dynamics. One of the possible way is to compute the *Hankel Singular Value* to understand which are the states that actually contribute to the control law. In fact, the Hankel Singular Value, σ is an indication of the energy associated to each state. Comparing them, it is possible to have an idea of the approximation order of the controller. The states with magnitude much more lower then others, for example four-five times lower, could be deleted. This is just a starting point, to have a general idea about what could be the reduced order. Therefore, after a first approximation, which could be done with *balred* (balanced reduction) the Bode diagram of the controllers have to be compared to verify that the frequency behaviour or the reduced and the original K is the same.

```
opts = hinfOptions('Method','LMI','Autoscale','on','Display','on')
k_red = balred(k,10,opt)
```

The *Model Reducer Application* of Matlab provides the equivalent functionalities, but it could result easier to handle thanks to the graphic interface e no need of scripting. Basically, the model to reduce has to be imported in the app, it is reduced according to the chosen strategy and then it is exported and saved. Choosing Balanced Truncation the app automatically reduces the model, otherwise the desired reduced order can be specified. Two plots are generated: a Bode diagram (magnitude and phase) of the two controller to compare the frequency behaviour of the reduced wrt the original.

The second plots the Hankel Singular Values, with an indication about which are the stable and unstable states.

Moreover, it is possible to set some constraints for the reduction. For example, the DC-gain of the model can be preserved or the truncation can be done only in a particular frequency range. It is also possible to reduce at different order

and compare all the controllers obtained. At the end the reduced model can be exported.

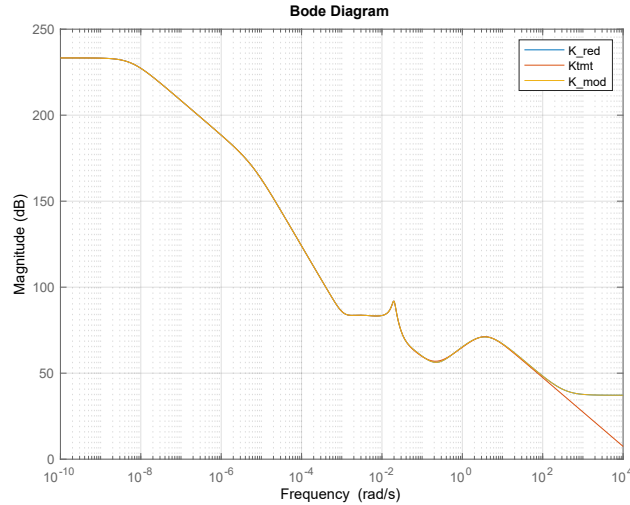


Figure 4.9: **Bode Diagram comparison of the reduced controllers.**

First it is checked if the reduced control law still satisfies the requirement in terms of transfer function. The same check of the figure 4.7 is performed. If it does, the controller is tested in the simulink enviroment. In the case the reduced controller does not meet the requirements in simulation, the reduction has to be rewied. Probably the reduction order is too low, an unstable pole has been deleted, or poles belonging to the frequency bandwidth of the system have been removed.

Chapter 5

Simulations

The controllers have been tested in a Simulink model implementing the whole system. Once the stability has been checked, then the performances are verified. The controllers are tested together being the system nonlinear and coupled. At first, a single simulation has been run to check the performance of the controllers. Once the desired behaviour has been reached, multiple simulations have been run to check its robustness.

5.1 Simulink set

The dynamics model of the system presented in the first chapter have been implemented in Simulink. An already existing model has been used and adapted to the MIMO case. The figure 5.1 shows the simulink model.

The main blocks of a general feedback control system can be identified:

- *Reference block*: all the reference signals of the variables are outputted from this block. It results to be a regulation problem, in fact all the references are at zero.

$$- \mathbf{q}_{SC} = \mathfrak{S} \doteq (1, \mathbf{0});$$

$$- \vec{\mathbf{r}}_{TMi} = 0;$$

$$- \theta_{TMi} = 0;$$

$$- \vec{\zeta}_{OA} = 0$$

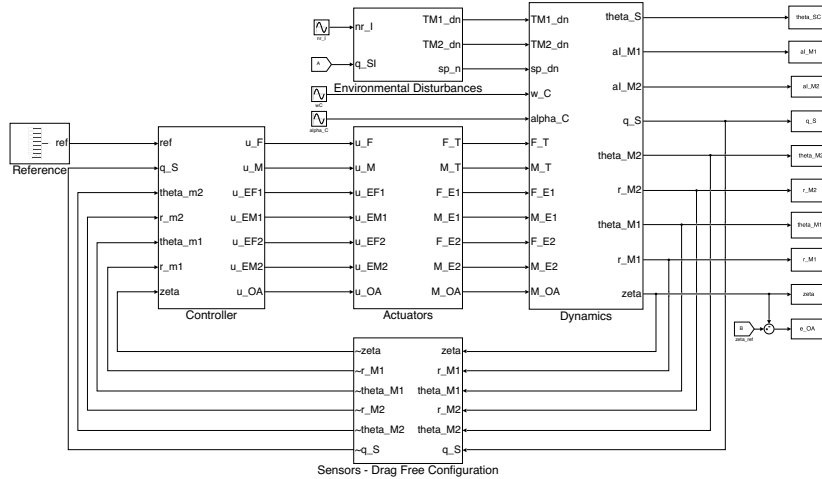


Figure 5.1: **Simulink scheme.**

- *Control Block:* the error signals are the input to the controllers that compute the command input u_i sent to the actuator blocks. It is clear from this block the mimo nature of the problem and also how the command inputs are obtained. A discretization of the controllers is needed before use them. The "Tustin" discretization method has been chosen, with a sampling time $T_s = 0.1$ s.
- *Plant:* the dynamics model of the system is implemented here;
- *Sensors block:* the outputs of the plant are filtered through the characteristic of the sensors, the measurement noise is added to the ideal output to obtain a more realistic one.

Moreover, the disturbances considered are: the Solar Pressure, which does not act at the geometrical center such that it creates a disturbance torques. The TMs are subject to the Self Gravity and enviromental disturbances, such as the Brownian. Furthermore actuator and sensor noises are present. All these contributions have been obtained as described in the first chapter, i.e. from a white noise colored by the noise shape filtered presented there.

The simulation has been run for a time $T_{fin} = 300000$ seconds with a sampling time $T_s = 0.1$ s, using the *ode23* solver.

Each output variable has been elaborated to obtain a periodogram, which is an expression of the spectral density of a signal. In particular the Welch spectral density estimate has been chosen to analyze the specification requirements, through *pwelch*.

The results of the simulation are listed in the next section.

5.2 Simulation results

At first the result of a single simulation are presented. All the requirements are referred to the frequency range specified by the *REQ DF-P-010* which set $f = [1e^{-5}; 1]Hz$.

First of all, the Drag Free direction is considered. Along the sensitive direction two performance requirements are set: an upper bound on the TMs position jitter and on the acceleration.

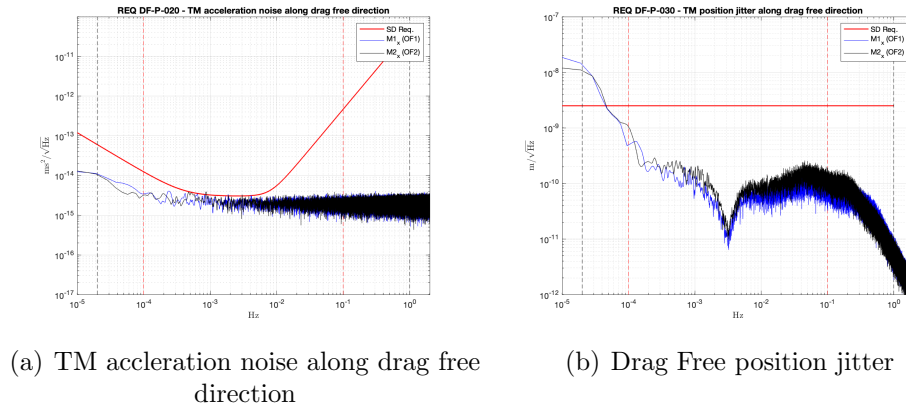


Figure 5.2: **Drag free position.**

The drag free inertial acceleration fulfills the requirement for all the specified frequency range, as shown in figure 5.2(a). This acceleration is caused by all the forces and disturbances acting on the TMs, i.e. the actuation forces, Brownian disturbance, static component and gradient of the Self gravity. The TMs jitter along x cross the bounds at $5.5e^{-4}$ Hz, fig. 5.2(b).

Figure 5.3 shows the other two degrees of freedom for the TMs translation.

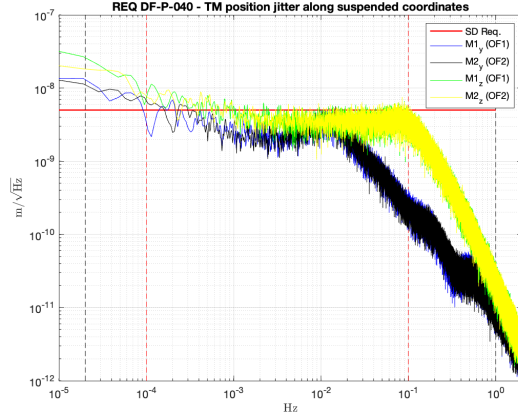
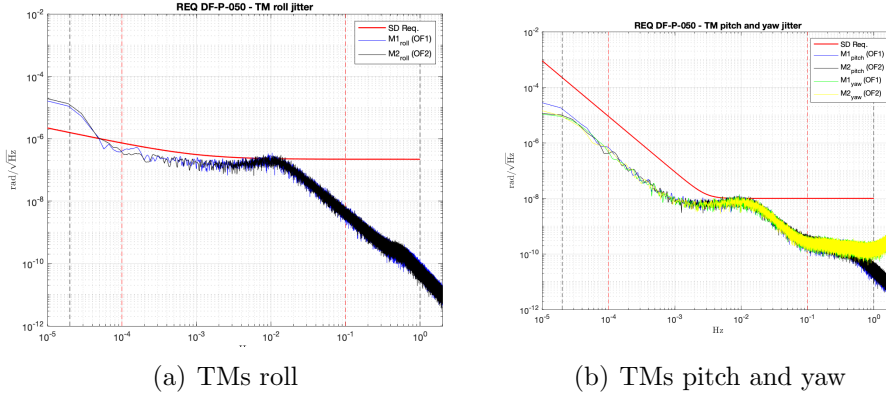


Figure 5.3: **TMs position jitter along y and z direction.**

Both the translation do not completely fulfill the requirement, in fact $rm_i(z)$ crosses the bound at $10^{-3}Hz$, $rm_i(y)$ slightly after at $10^{-4}Hz$. This was expected, because it reflects the shapes of the functions during the design. This misbehaviour is caused by high measurement noise introduced in the feedback.

The TMs attitude instead fulfill all the requirements, even though the roll loop has high sensing noise, fig. 5.4



(a) TMs roll

(b) TMs pitch and yaw

Figure 5.4: **Test Mass attitude.**

At least, the spacecraft attitude jitter and the optical assembly angle variation fulfill the requirements, fig. 5.5

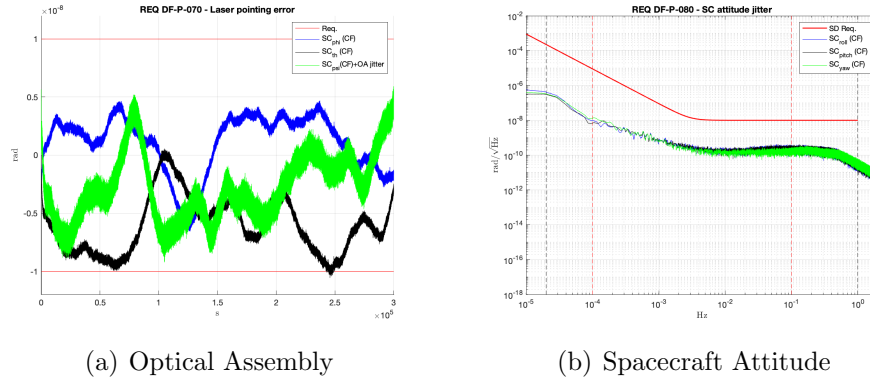


Figure 5.5: Spacecraft attitude and OA.

Both the requirement are satisfied.

5.3 Monte Carlo Simulation and Results

One of the most important property of a control system is robustness. It refers to the property of a system to be robust against uncertainties, i.e. the control law has to unsure stability and fulfill requirements even in the presence of uncertainty affecting the system. In fact, any system can not be exactly known, because of parametric uncertainty. This can be related to poor accuracy of the model, neglected dynamics or the presence of disturbances which can not be exactly modelled. In this case study, the uncertainties are mainly related to some unmodelled dynamics and disturbances. To cope with this source of uncertainties and test the controller robustness, Monte Carlo Simulations have been run.

All the previous coefficients are estimated experimentally, so they will be affected by uncertainty. Mass and inertia are affected by uncertainty too, moreover they are also time-varying parameters since mass decreases over time due to propellant consumption, consequently the inertia tensor changes, as well as the self-gravity gradient.

Actuation and sensing noises have been already discussed in chapter 4. Another important source of disturbances is given by neglected dynamics. Many devices are difficult to model, therefore simpler first or second order models are used in the control algorithms.

Monte Carlo method is an algorithm which relies on repeated random samplings and probability distributions to obtain numerical results. It is used to randomly initialized parameters that are sources of uncertainty and disturbances. In this case, only the parameters affected by high uncertainties have been randomized, due to computational limits of a computer simulation.

It is used as a posteriori validation method. In fact, the control robustness is tested by randomly initializing uncertain parameters and disturbs affecting the plant. The parameter randomized in this case are:

- Spacecraft mass and inertia matrix: change during the mission due to fuel consumption;
- Self Gravity: it is the main source of unmodelled uncertainty dynamics, although it has been modelled has a spring force and coupling between test masses and spacecraft, the entries of the matrix are affected by high uncertainty, both in terms of static component of forces and torques;
- stiffness matrix;

The parameters are randomly initialized in a Matlab scripts and the each simulation is run in Simulink, for a $T_{sim} = 300000$ s. The results are collected, then stability and performances are checked. The former is verified computing the H_{∞} norm and the square norm of the variable, which has to be lower than a defined tolerance value. The latter is checked comparing the pwelch of the variable with the frequency expression of the requirements.

`pxx = pwelch(x)` returns the power spectral density (PSD) estimate, `pxx`, of the input signal, `x`, found using Welch's overlapped segment averaging estimator. When `x` is a vector, it is treated as a single channel. When `x` is a matrix, the PSD is computed independently for each column and stored in the corresponding column of `pxx`. If `x` is real-valued, `pxx` is a one-sided PSD estimate. If `x` is complex-valued, `pxx` is a two-sided PSD estimate. By default, `x` is divided into the longest possible segments to obtain as close to but not exceed 8 segments with 50 percent overlap. Each segment is windowed with a Hamming window. The modified periodograms are averaged to obtain the PSD estimate. If you cannot divide the length of `x` exactly into an integer number of segments with 50

In this case 50 simulations have been run. The output data have been collected and elaborated through a dedicated Matlab script that generates three tables. In the first one, there are listed all the variables and the corresponding simulation number. If all the states are stable, at the simulation is associated 1, otherwise 0. The second and third table respectively shows the percentage of error crossing the bound and the maximum error at the corresponding frequency for each variable for all the simulation.

However, a quick overview of the results is provided by two percentages. The simulations were stable in the 99.33% of cases, while the performance requirements were satisfied in the 92.1%.

Chapter 6

Conclusions

This thesis aimed at the design of drag-free controllers for a space-based gravitational wave observatory like LISA.

The control problem consisted in the simultaneous control of 20 degrees of freedom, with demanding performance requirements and relatively high actuation, sensing and environmental noises. After the study of the plant, a MIMO mixed sensitivity loop shaping approach appeared to be a suitable choice, because it involves the noise and the requirements shapes in the definition of the weighting functions. Although this could be a good starting point for the design, it also counteracts the need of high loop gain at low frequency to reach good reference tracking and disturbance rejection.

After the design phase a Monte Carlo campaign of 50 simulations was performed to test the controllers robustness and requirements feasibility.

Parameters affected by uncertainty and those ones varying along the mission have been randomized around some reference value. There were the mass and inertia matrix of the spacecraft, stiffness matrix, self gravity contributions and disturbances affecting the masses.

Hence, the H_∞ and H_2 norms of the output variables have been computed to check the stability.

For what concerns the performances, the power spectral density of the variable of interest were computed and compared with the corresponding requirement.

It was found that some requirements resulted to be unfeasible below a specific

frequency value, which can be demonstrated as reported in [14], mainly caused by the high actuation and sensing noises entering the system.

The drag free coordinates is unfeasible below $5 \cdot 10^{-5} Hz$, the z -translation cross the bound at $1 \cdot 10^{-3}$ while the y -translation at $1 \cdot 10^{-4} Hz$. Also the test mass roll results to be unfeasible already between $[6 \cdot 10^{-3} 5 \cdot 10^{-1}] Hz$.

The percentage of stability success is 99.33%, while the performance success is 92.1%.

The campaign confirmed the stability of the controllers and its robustness, without considering the unfeasible frequency range known a priori.

In order to cope with this scenario, a possible solution could be relaxing the requirements as long as the Gravitational Waves detection is not compromised. Otherwise, less noise sensors are needed.

Bibliography

- [1] James Hough, Sheila Rowan, and Bangalore Sathyaprakash. The search for gravitational waves. *Journal of Physics B Atomic Molecular and Optical Physics*, 38, 01 2005. doi: 10.1088/0953-4075/38/9/004.
- [2] EADS Astrium. Cutaway view of a lisa spacecraft. 2010. URL https://sci.esa.int/web/lisa/display-page-display-page-default/-/asset_publisher/35015/content/46428-cutaway-view-of-a-lisa-spacecraft.
- [3] EADS Astrium. Lisa telescope design. 2007. URL <https://sci.esa.int/web/lisa/-/41273-lisa-telescope-design>.
- [4] Mathworks. Loop shaping of himat pitch axis controller. 2009. URL <https://it.mathworks.com/help/robust/examples/loop-shaping-of-himat-pitch-axis-controller.html>.
- [5] Mathworks. augm. URL <https://it.mathworks.com/help/robust/ref/lti.augw.html>.
- [6] Dennis Weise Peter F. Gath, Hans Reiner Schulte and Ulrich Johann. Drag free and attitude control system design for the lisa science mode, eads astrium gmbh. *American Institute of Aeronautics and Astronautics, Inc*, 08 207.
- [7] Katsuhiko Ogata. Prentice Hall, New Jersey, 2010. ISBN 0-13-615673-8.
- [8] Giuseppe Racca Paul McNamara. Introduction to lisa pathfinder. 2009. ISSN LISA-LPF-RP-0002.
- [9] S. Vidano. The lisa dfacs a nonlinear model for the spacecraft dynamics. *Aerospace Science and Technology*, 2020.

- [10] C. Novara. Assessment and preliminary prototyping of a drag free control system for the l3 gravity wave observatory. *Politecnico di Torino*, 2018.
- [11] F.B.J.W.M. Hendriks. High performance robust control, system identification, and model validation: A literature study. 10 2008. doi: DCT2008.143.
- [12] Roland Longchamp Gorka Galdos, Alireza Karimi. H infinity controller design for spectral mimo models by convex optimization. *Journal of Process Control*, 08 2010.
- [13] Mathworks. Loop shaping of himat pitch axis controller. 2009. URL <https://it.mathworks.com/help/robust/gs/using-mixsyn-for-h-infinity-loop-shaping.html>.
- [14] S.Vidano C. Novara. Decoupling and mixed sensitivity h-inf control design for the lisa drag free mode, technical note. *Politecnico di Torino*, 2020.